Test of many-body methods on an exactly soluble model with backbending and gapless superconductivity*

S. Y. Chu, E. R. Marshalek,† P. Ring,‡ J. Krumlinde,§ and J. O. Rasmussen
Lawrence Berkeley Laboratory, University of California, Berkeley, California 94720
(Received 24 April 1975)

The exactly soluble R(8) model of Krumlinde and Szymański is used as a testing ground for three many-body methods applied to the yrast band: (i) the self-consistent cranking model, (ii) self-consistent cranking plus random-phase approximation, and (iii) variation after projection of particle number. All three methods agree very well with exact results outside of the critical region. The behavior in the critical region is examined in detail.

[NUCLEAR STRUCTURE Many-body methods, solvable model, high-spin states.]

I. INTRODUCTION

The peculiar behavior of the nuclear moment of inertia at high spin has elicited considerable experimental and theoretical efforts in recent years.[1] Among microscopic theories, Hartree-Bogoliubov self-consistent cranking (SCC) calculations[2] (and approximations to such calculations[3]) have been especially successful in accounting for the sharp increase in the moment of inertia, "backbending," and "gapless superconductivity"[4] in realistic cases. The SCC method has the virtues of greater simplicity and speed in comparison with shell-model calculations with the same Hamiltonian and yet is rich enough to encompass all the possible mechanisms which may contribute to the behavior of the moment of inertia at high spin, such as Coriolis antipairing and realignment (decoupling), gapless superconductivity, band mixing, and changes in shape. Nevertheless, this technique has some potentially serious deficiencies. First, it is basically a classical approximation, and, second, the cranked wave functions violate symmetries (e.g., conservation of angular momentum and particle number), the two aspects being related, as is well known.

The classical aspect should not be a shortcoming at sufficiently high spin, but it must be kept in mind that this is only so in regions well removed from "phase transitions," since in critical regions quantum fluctuations may become very large. Actually, there exist proofs of the validity of SCC both at low and very high spins, but these make use of infinite power-series expansions in the angular momentum, which cannot be expected to converge in critical regions.[5] The violation of symmetries in the wave functions renders difficult the calculation of the transition amplitudes.

Projection of particle number and angular momentum before variation is one possible remedy for the above difficulties. Another, recently proposed remedy, is the inclusion of random-phase approximation (RPA) correlations as the next improvement to the SCC model (SCC + RPA).[6] As is well known, the RPA maintains the conservation laws to the order of the approximation. Both methods introduce quantal correlation effects.

Our first aim in this paper is to shed light on these questions by testing the three approximations: SCC, SCC + RPA, and variation after projection of particle number (VAPN), on the "exactly soluble" R(8) model of Krumlinde and Szymański.[7,8] The SCC + RPA method has been previously successfully tested on the R(5) model,[6] but that is only a two-dimensional model, whereas the R(8) model is three-dimensional. Our second aim is to illustrate how transition probabilities can be simply calculated in the SCC + RPA framework, a procedure which can be easily extended to realistic cases.

II. DESCRIPTION OF THE MODELS

A. R(8) model

The R(8) model consists of 2Ω identical fermions interacting via a pairing force, distributed among two 2Ω-fold degenerate single-particle levels separated by the energy 2ϵ and coupled to an external rotor with fixed moment of inertia a^{-1}. The Hamiltonian is

$$H = (\tfrac{1}{2}a)|\vec{I}-\vec{j}|^2 + H_{\text{s.p.}} + H_{\text{p}}, \tag{2.1}$$

where $\vec{I}$ is the total angular momentum of the system, and $\vec{j}$ is the particle angular momentum. The single-particle Hamiltonian $H_{\text{s.p.}}$ is given by

$$H_{\text{s.p.}} = \epsilon \sum_{\nu=1}^{\Omega} (a_\nu^\dagger a_\nu + a_{\bar{\nu}}^\dagger a_{\bar{\nu}} - b_\nu^\dagger b_\nu - b_{\bar{\nu}}^\dagger b_{\bar{\nu}}), \tag{2.2}$$

while H_p is the pairing interaction of strength G:

$$H_p = -G \sum_{\nu=1}^{\Omega} (a_\nu^\dagger a_{\bar\nu}^\dagger + b_\nu^\dagger b_{\bar\nu}^\dagger) \sum_{\nu=1}^{\Omega} (a_{\bar\nu} a_\nu + b_{\bar\nu} b_\nu). \tag{2.3}$$

The operator $a_\nu^\dagger$ creates a fermion in the upper level and $b_\nu^\dagger$ in the lower level, while $a_{\bar\nu}^\dagger$ and $b_{\bar\nu}^\dagger$ are the corresponding time-reversal conjugate operators: $a_{\bar\nu}^\dagger = T a_\nu^\dagger T^{-1}$, $b_{\bar\nu}^\dagger = T b_\nu^\dagger T^{-1}$. The particle angular momenta as defined by Krumlinde and Szymański are

$$j_+ = j_x + i j_y = (3)^{1/2} \sum_{\nu=1}^{\Omega} (a_\nu^\dagger b_\nu - b_{\bar\nu}^\dagger a_{\bar\nu}) + 2 \sum_{\nu=1}^{\Omega} b_\nu^\dagger b_{\bar\nu}, \tag{2.4a}$$

$$j_- = j_+^\dagger,$$

$$j_z = \frac{3}{2} \sum_{\nu=1}^{\Omega} (a_\nu^\dagger a_\nu - a_{\bar\nu}^\dagger a_{\bar\nu}) + \frac{1}{2} \sum_{\nu=1}^{\Omega} (b_\nu^\dagger b_\nu - b_{\bar\nu}^\dagger b_{\bar\nu}). \tag{2.4b}$$

This corresponds to assigning the z projection $K = \frac{3}{2}$ for the upper levels and $K = \frac{1}{2}$ for the lower levels.

As discussed in Ref. 8, H is composed of generators of the group R(8). Exact eigenvalues and eigenfunctions can be found by diagonalizing a matrix in the Gelfand basis, so that the exact solution corresponds to a prototype shell-model calculation.

We note that the particle Hamiltonian $H_{\text{s.p.}} + H_p$ in this model does not commute with $\vec{j}$. The total angular momentum $\vec{I}$ is conserved only because the particles are coupled to an external rotor (which simulates a core). For this reason, it is not meaningful to test angular momentum projection on the R(8) model.

As a final point, we shall restrict the space of the model to the representation of R(8) containing the ground state.

B. Self-consistent cranking model

Before deriving the SCC model, it is convenient to perform a simple unitary transformation due to Goodman.[9] The purpose is to eliminate matrix elements of j_x between time-reverse conjugate states, which, in turn, halves the dimension of the Hartree-Bogoliubov matrix. We introduce new fermion operators $(\tilde a, \tilde a^\dagger, \tilde b, \tilde b^\dagger)$ defined by

$$\tilde a_\nu^\dagger = (2)^{-1/2}(a_\nu^\dagger - a_{\bar\nu}^\dagger), \quad \tilde a_{\bar\nu}^\dagger = (2)^{-1/2}(a_\nu^\dagger + a_{\bar\nu}^\dagger),$$
$$\tilde b_\nu^\dagger = (2)^{-1/2}(b_\nu^\dagger + b_{\bar\nu}^\dagger), \quad \tilde b_{\bar\nu}^\dagger = -(2)^{-1/2}(b_\nu^\dagger - b_{\bar\nu}^\dagger). \tag{2.5}$$

This transformation leaves $H_{\text{s.p.}}$ and H_p invariant:

$$H_{\text{s.p.}}(a^\dagger, a, b^\dagger, b) = H_{\text{s.p.}}(\tilde a^\dagger, \tilde a, \tilde b^\dagger, \tilde b),$$
$$H_p(a^\dagger, a, b^\dagger, b) = H_p(\tilde a^\dagger, \tilde a, \tilde b^\dagger, \tilde b). \tag{2.6}$$

The angular momenta take the following form:

$$j_x = \tfrac{1}{2}(3)^{1/2} \sum_{\nu=1}^{\Omega} (\tilde a_\nu^\dagger \tilde b_\nu - \tilde b_{\bar\nu}^\dagger \tilde a_{\bar\nu} + \text{H.c.}) + \sum_{\nu=1}^{\Omega} (\tilde b_\nu^\dagger \tilde b_\nu - \tilde b_{\bar\nu}^\dagger \tilde b_{\bar\nu}),$$

$$j_y = -i\tfrac{1}{2}(3)^{1/2} \sum_{\nu=1}^{\Omega} (\tilde a_{\bar\nu}^\dagger \tilde b_\nu - \tilde a_\nu^\dagger \tilde b_{\bar\nu} - \text{H.c.}) - i \sum_{\nu=1}^{\Omega} (\tilde b_\nu^\dagger \tilde b_{\bar\nu} - \tilde b_{\bar\nu}^\dagger \tilde b_\nu), \tag{2.7}$$

$$j_z = \frac{3}{2} \sum_{\nu=1}^{\Omega} (\tilde a_\nu^\dagger \tilde a_{\bar\nu} + \tilde a_{\bar\nu}^\dagger \tilde a_\nu) - \frac{1}{2} \sum_{\nu=1}^{\Omega} (\tilde b_\nu^\dagger \tilde b_{\bar\nu} + \tilde b_{\bar\nu}^\dagger \tilde b_\nu).$$

Matrix elements of j_x between time-reverse conjugate states, are now replaced by diagonal matrix elements, which is sufficient to reduce the dimension.

In the case of a self-contained many-fermion system with Hamiltonian H, the SCC model is usually derived by applying Hartree-Bogoliubov factorization to the operator $H - \omega j_x$. With the R(8) model, there is no need to subtract ωj_x since the rotor already cranks the system. Instead, we assume in the first approximation that the total angular momentum is aligned in the x direction and has the classical c-number value I:

$$I_x \approx I, \quad I_y \approx 0, \quad I_z \approx 0. \tag{2.8}$$

Subsequently, Hartree-Bogoliubov factorization of H yields the SCC Hamiltonian H_ω:

$$H_\omega = \mathcal{E}_0(\omega) + :H_{\text{s.p.}} - \Delta \sum_{\nu=1}^{\Omega} (\tilde a_\nu^\dagger \tilde a_{\bar\nu}^\dagger + \tilde b_\nu^\dagger \tilde b_{\bar\nu}^\dagger + \text{H.c.}) - \omega j_x : . \tag{2.9}$$

The terms embraced by the symbol : : are to be regarded as normal ordered with respect to the vacuum state of H_ω, the energy being given by

$$\mathcal{E}_0(\omega) = \langle H_{\text{s.p.}} \rangle_\omega - \Delta^2/G + \tfrac{1}{2} a (I - \langle j_x \rangle_\omega)^2, \tag{2.10}$$

where $\langle\ \rangle_\omega$ denotes the expectation value with respect to the vacuum of H_ω. The gap parameter Δ and the angular frequency ω are determined by the self-consistency conditions

$$\Delta = G \sum_{\nu=1}^{\Omega} (\langle \tilde a_{\bar\nu} \tilde a_\nu \rangle_\omega + \langle \tilde b_{\bar\nu} \tilde b_\nu \rangle_\omega) \tag{2.11}$$

and

$$\frac{\omega}{a} = I - \langle j_x \rangle_\omega . \tag{2.12}$$

There are also the requirements

$$\langle j_y \rangle_\omega = \langle j_x \rangle_\omega = 0 , \tag{2.13}$$

which are fulfilled automatically.

The form of the SCC model derived above, which shall be specifically referred to as SCC1, is purely classical, and as such, valid mainly for high values of I. For low values of I, the rotational energy goes as I^2 rather than $I(I+1)$.[10] However, the addition of quantum fluctuations arising from the RPA, to be discussed later, gives the correct $I(I+1)$ dependence. If RPA corrections are *not* included, the cranking energy may be improved for low I by directly modifying (2.12) as follows:

$$\frac{\omega}{a} = [I(I+1)]^{1/2} - \langle j_x \rangle_\omega . \tag{2.14}$$

This version of self-consistent cranking, which corresponds to the usual procedure, shall be called SCC2.

Let us briefly consider the problem of diagonalizing the fermion quadratic form H_ω. This is simplified, first of all, by the fact that H_ω is the sum of Ω identical quadratic forms, and, second, by the fact that the chemical potential vanishes independently of ω, which is a consequence of the fact that the number of particles is half the available number of levels. H_ω can be brought into the diagonal form

$$H_\omega = \mathcal{E}_0(\omega) + \sum_{i=1}^{4} E_i \sum_{\nu=1}^{\Omega} \alpha_\nu^\dagger(i)\alpha_\nu(i) , \tag{2.15}$$

where the $\alpha_\nu^\dagger(i)$ are independent quasiparticle creation operators related to the particle operators by the Bogoliubov transformation

$$\begin{aligned} \alpha_\nu^\dagger(i) &= U_{1i}\tilde{a}_\nu^\dagger + U_{2i}\tilde{b}_\nu^\dagger + V_{3i}\tilde{b}_{\bar{\nu}} + V_{4i}\tilde{a}_{\bar{\nu}}, \quad i = 1, 2 , \\ \alpha_\nu(i) &= V_{1i}\tilde{a}_\nu^\dagger + V_{2i}\tilde{b}_\nu^\dagger + U_{3i}\tilde{b}_{\bar{\nu}} + U_{4i}\tilde{a}_{\bar{\nu}}, \quad i = 3, 4 , \end{aligned} \tag{2.16}$$

where the U's and V's are independent of the index ν, and correspond to the eigenvectors of a 4×4 matrix with eigenvalues E_i, $i=1,2$ and $-E_i$, $i=3,4$. If it were not for the Goodman transformation (2.5), one would have to deal with an 8×8 matrix.

The quasiparticle energies explicitly are

$$\begin{aligned} E_1 &= -\tfrac{1}{2}\omega + E_-, \quad E_2 = -\tfrac{1}{2}\omega + E_+ , \\ E_3 &= \tfrac{1}{2}\omega + E_-, \quad E_4 = \tfrac{1}{2}\omega + E_+ , \end{aligned} \tag{2.17}$$

where

$$E_\pm = (\epsilon^2 + \Delta^2 + \omega^2 \pm \omega\gamma)^{1/2} \tag{2.18}$$

and

$$\gamma = (\epsilon^2 + 4\Delta^2)^{1/2} . \tag{2.19}$$

The coefficients of the Bogoliubov transformation are explicitly the following. Define

$$F_\pm(\epsilon, \omega) = \left\{ \frac{(\gamma+\epsilon)[\gamma + 2\omega + 3\epsilon \pm 4e(\omega)]}{\pm 16\gamma e(\omega)} \right\}^{1/2} , \tag{2.20}$$

where

$$e(\omega) = E_+ . \tag{2.21}$$

Then

$$\begin{aligned} &U_{11} = -V_{23} = F_-(-\epsilon, -\omega), \quad U_{21} = V_{13} = \sigma_+ F_+(-\epsilon, -\omega), \\ &V_{31} = -U_{43} = -F_+(\epsilon, -\omega), \quad V_{41} = U_{33} = -\sigma_- F_-(\epsilon, -\omega), \\ &U_{12} = V_{24} = -F_+(\epsilon, \omega), \quad U_{22} = -V_{14} = F_-(\epsilon, \omega), \\ &V_{32} = U_{44} = -F_-(-\epsilon, \omega), \quad V_{42} = -U_{34} = F_+(-\epsilon, \omega), \end{aligned} \tag{2.22}$$

in which $\sigma_\pm$ is a phase factor given by

$$\sigma_\pm = \mathrm{sgn}[\gamma - 2\omega \pm e(-\omega)] . \tag{2.23}$$

With the aid of the Bogoliubov transformation (2.16), and (2.22), one obtains from (2.11) the simple gap equation

$$\frac{G\Omega}{2\gamma}\left(\frac{\gamma+2\omega}{E_+} + \frac{\gamma-2\omega}{E_-}\right) = 1 , \tag{2.24}$$

which determines Δ as a function of ω.

Similarly, (2.12) or (2.14) determine the relation between I and ω:

$$J = \frac{\omega}{a} + \langle j_x \rangle_\omega = \frac{\omega}{a} + \frac{\Omega}{2}\left(\frac{\gamma+2\omega}{E_+} - \frac{\gamma-2\omega}{E_-}\right) , \tag{2.25}$$

where J is defined as follows:

$$J = I \quad \text{(SCC1)}, \tag{2.26a}$$

$$J = [I(I+1)]^{1/2} \quad \text{(SCC2)} . \tag{2.26b}$$

The moment of inertia is defined as usual by

$$\mathcal{J} = J/\omega . \tag{2.27}$$

The total cranking energy (2.10) has the explicit value

$$\mathcal{E}_0(\omega) = \frac{-\epsilon^2\Omega}{2\gamma}\left(\frac{2\gamma+\omega}{E_+} + \frac{2\gamma-\omega}{E_-}\right) - \frac{\Delta^2}{G} + \frac{\omega^2}{2a} , \tag{2.28}$$

with ω related to I through (2.25) and (2.26).

Finally, we call attention to the feature of "gapless superconductivity" in this model. For $|\omega|$ greater than a critical value $\omega_1 = \frac{2}{3}[\gamma_1 - (\Delta_1^2 - 2\epsilon^2)^{1/2}]$, the quasiparticle energy E_1 may turn negative (this can only happen for E_1), while the order pa-

rameter $\Delta \neq 0$. At a larger value $\omega_2 = \frac{2}{3}[\gamma_2 + (\Delta_2{}^2 - 2\epsilon^2)^{1/2}]$, E_2 may again turn positive. (It is necessary of course that $\Delta^2 - 2\epsilon^2 > 0$ at these two points for the behavior to occur.) The name of the phenomenon derives from the consequent disappearance of the gap in the excitation spectrum. In realistic calculations, it seems that only one quasiparticle energy turns negative. Since the spectrum of an even-fermion system requires creation of at least two quasiparticles in different states, the excitation energies remain positive. The artificial degeneracy of the R(8) model, however, poses a special problem, since a state $\alpha_\nu^\dagger(1)\alpha_{\nu'}^\dagger(1)|\omega\rangle$, $\nu \neq \nu'$ ($|\omega\rangle$ is the quasiparticle vacuum) can be created with energy $2E_1 < 0$ etc.[10(a)] The restriction of the space of the model to a single representation of R(8) containing the ground state, however, rules out the troublesome quasiparticle states and the behavior is more like that of the realistic cases. We note that the gapless superconductivity arises from the $K = \frac{1}{2} \rightarrow K = -\frac{1}{2}$ matrix elements of j_x, i.e., the term $2\sum_\nu b_\nu^\dagger b_{\bar{\nu}}$ in (2.4a). Omission of this term would leave all quasiparticle energies nonnegative.

C. Self-consistent cranking plus RPA

We now consider the corrections to SCC1 described by the RPA. The boson-expansion technique provides a convenient way to introduce the additional correlations. Boson expansions to all orders for the group $R(2n)$ have been given in Ref. 11. In the present problem, H must first be expressed in terms of the quasiparticles (2.16). Then, the quasiparticle pair operators are expanded in bosons to the RPA order as follows:

$$\sum_{\nu=1}^{\Omega} \alpha_\nu^\dagger(i)\alpha_\nu^\dagger(j) \approx \Omega^{1/2} B_{ij}^\dagger , \tag{2.29a}$$

$$\sum_{\nu=1}^{\Omega} \alpha_\nu^\dagger(i)\alpha_\nu(i) = \sum_j B_{ij}^\dagger B_{ij} , \tag{2.29b}$$

where the $B_{ij}, B_{ij}^\dagger$ are boson operators obeying the usual commutation rules

$$[B_{ij}, B_{kl}] = 0 , \quad [B_{ij}, B_{kl}^\dagger] = \delta_{ik}\delta_{jl} - \delta_{il}\delta_{jk} , \tag{2.30}$$

and the antisymmetry condition $B_{ji} = -B_{ij}$.

Equation (2.29a) omits terms of order $\Omega^{-1/2}$ (anharmonic corrections), while the finite expression (2.29b) is exact. Note that only those boson degrees of freedom are included which are relevant to the single representation of R(8) with which we are concerned.

It turns out to be convenient to make the following change of phase:

$$B_{12}^\dagger \rightarrow iB_{12}^\dagger , \quad B_{34}^\dagger \rightarrow iB_{34}^\dagger , \tag{2.31}$$

as will be seen later.

In addition to the particles, the core must also be expanded in bosons, which physically corresponds to its wobbling motion about the steady rotation. A full description of the boson representation of a quantized rotor, with expressions valid to all orders, is given in Ref. 12. We follow here the lowest-order treatment originally applied by Bohr and Mottelson to the asymmetric rotor,[13] which is applicable to the symmetric rotor as well. The body-fixed components of the total angular momentum are given by

$$I_+ = I_y + iI_z \approx (2I)^{1/2} b^\dagger , \qquad I_- = I_y - iI_z \approx (2I)^{1/2} b , \tag{2.32a}$$

$$I_x = I - b^\dagger b . \tag{2.32b}$$

Equation (2.32a) omits terms of order $I^{-1/2}$, while (2.32b) is exact. We see that these include the small-oscillation correction to the classical ansatz (2.8). The core bosons commute, of course, with the particle bosons:

$$[b, B_{ij}] = [b, B_{ij}^\dagger] = 0 . \tag{2.33}$$

In the boson representation, the Hartree-Bogoliubov Hamiltonian H exactly takes the form

$$H_\omega = \mathcal{E}_0(\omega) + \frac{1}{2}\sum_{ij} (E_i + E_j) B_{ij}^\dagger B_{ij} . \tag{2.34}$$

Upon adding the RPA correlations, one finds that the total Hamiltonian breaks up into two disjoint quadratic boson forms:

$$H \approx H_{\mathrm{RPA}} = \mathcal{E}_0(\omega) + H_3 + H_4 . \tag{2.35}$$

H_3 is given by

$$H_3 = -\omega b^\dagger b + (E_+ + E_- - \omega) B_{12}^\dagger B_{12} + (E_+ + E_- + \omega) B_{34}^\dagger B_{34} + \tfrac{1}{2} a (I_y^{(1)} - j_y^{(1)})^2 + \tfrac{1}{2} a (I_z^{(1)} - j_z^{(1)})^2 , \tag{2.36}$$

where

$$I_y^{(1)} = (\tfrac{1}{2}I)^{1/2}(b^\dagger + b) , \qquad I_z^{(1)} = i(\tfrac{1}{2}I)^{1/2}(b - b^\dagger) , \tag{2.37a}$$

and

$$\begin{aligned} j_y &\approx j_y^{(1)} \\ &= k[(E_+ + E_- - \omega)(E_+ + E_- + 2\omega)(B_{12}^\dagger + B_{12}) \\ &\quad - (E_+ + E_- + \omega)(E_+ + E_- - 2\omega)(B_{34}^\dagger + B_{34})] , \\ j_z &\approx j_z^{(1)} = ik\omega[(E_+ + E_- + 2\omega)(B_{12}^\dagger - B_{12}) \\ &\quad - (E_+ + E_- - 2\omega)(B_{34}^\dagger - B_{34})] , \end{aligned} \tag{2.37b}$$

and the factor k is given by

$$k=\tfrac{1}{2}(E_{+}+E_{-})^{-3/2}\quad(\langle j_x\rangle_\omega/\omega)^{1/2}. \tag{2.38}$$

Note that $\langle j_x\rangle_\omega/\omega=\mathcal{I}-a^{-1}$ is just the particle contribution to the moment of inertia and remains finite as $\omega\to 0$.

The three-boson quadratic form H_3 takes into account the wobbling of the rotor and its coupling to the particles and also the fluctuations of j_y and j_z away from the values (2.13).

The four-boson quadratic form H_4 is given by

$$H_4=(E_{+}+E_{-})(B^{\dagger}_{14}B_{14}+B^{\dagger}_{23}B_{23})+2E_{+}B^{\dagger}_{24}B_{24}+2E_{-}B^{\dagger}_{13}B_{13}+\tfrac{1}{2}a(j_x^{(1)})^2-GP^{(1)\dagger}P^{(1)}, \tag{2.39}$$

where

$$j_x-\langle j_x\rangle_\omega\approx j_x^{(1)}=\tfrac{1}{2}(3\Omega)^{1/2}\epsilon\left[\frac{1}{E_{+}}(B^{\dagger}_{24}+B_{24})-\frac{1}{E_{-}}(B^{\dagger}_{13}+B_{13})\right] \tag{2.40}$$

and $P^{(1)}$ is the fluctuation of the pair-transfer operator about the value Δ/G given by

$$P^{(1)}=\frac{(3\Omega)^{1/2}\epsilon\Delta}{2\gamma}\left[\frac{1}{E_{+}}(B^{\dagger}_{24}+B_{24})+\frac{1}{E_{-}}(B^{\dagger}_{13}+B_{13})\right]+\left[\frac{\Omega(E_{+}+E_{-})}{16\gamma^3}\left(\frac{\gamma+2\omega}{E_{+}}+\frac{\gamma-2\omega}{E_{-}}\right)\right]^{1/2}\times[(\gamma-\epsilon)(B^{\dagger}_{23}-B_{14})+(\gamma+\epsilon)(B^{\dagger}_{14}-B_{23})]. \tag{2.41}$$

It is useful to note from (2.24) that

$$\left[\frac{\Omega(E_{+}+E_{-})}{16\gamma^3}\left(\frac{\gamma+2\omega}{E_{+}}+\frac{\gamma-2\omega}{E_{-}}\right)\right]^{1/2}=\left(\frac{E_{+}+E_{-}}{8G\gamma^2}\right)^{1/2}\quad(\text{for }\Delta\neq 0). \tag{2.42}$$

H_4 describes pair vibrations and rotations and the fluctuations in j_x about the value $\langle j_x\rangle_\omega$.

We shall consider briefly the diagonalization of the quadratic forms in terms of normal modes. Further details are given in the Appendix. In the case of H_3, one finds two nonzero-frequency modes and one zero-frequency mode. The latter arises from the fact that I_z-j_z is a constant of the motion:

$$[H, I_z-j_z]=0. \tag{2.43}$$

Correspondingly, in the RPA, one must have

$$[H_3,(I_z-j_z)^{(1)}]=0, \tag{2.44}$$

where

$$(I_z-j_z)^{(1)}=I_z^{(1)}-j_z^{(1)}=-i(\tfrac{1}{2}I)^{1/2}(b^{\dagger}-b)-j_z^{(1)}. \tag{2.45}$$

The technique of Ref. 14 for treating zero-frequency normal modes leads to the quadratic form

$$H_3=\mathcal{E}_3(\mathrm{zp})+\sum_{\sigma=1}^{2}\omega_{3\sigma}\Theta^{\dagger}_{3\sigma}\Theta_{3\sigma}+\tfrac{1}{2}(I_z-j_z)^{(1)2}/M_3, \tag{2.46}$$

where M_3 is an "inertial parameter" associated with the zero-frequency mode. The operator $\Theta^{\dagger}_{3\sigma}$ is a boson creation operator for a vibrational normal mode with frequency $\omega_{3\sigma}$. It can be expressed as a linear combination of the original bosons:

$$\Theta^{\dagger}_{3\sigma}=X(3\sigma)b^{\dagger}+Y(3\sigma)b+X_{12}(3\sigma)B^{\dagger}_{12}+Y_{12}(3\sigma)B_{12}+X_{34}(3\sigma)B^{\dagger}_{34}+Y_{34}(3\sigma)B_{34}, \tag{2.47}$$

where the X's and Y's are RPA amplitudes. The energy of the zero-point oscillations is $\mathcal{E}_3(\mathrm{zp})$.

In the case of H_4, one must distinguish between the two situations $\Delta\neq 0$ and $\Delta=0$. If $\Delta\neq 0$, Eq. (2.42) applies and there are three nonzero-frequency modes and one zero-frequency mode, which is the so-called pairing rotation, arising from conservation of particle number $\hat{N}$:

$$[H,\hat{N}]=0. \tag{2.48}$$

Correspondingly, in the RPA, we have

$$[H_4,\hat{N}^{(1)}]=0, \tag{2.49}$$

where $\hat{N}^{(1)}$ is the linear boson approximation to $\hat{N}$. The Hamiltonian can then be written in the form

$$H_4=\mathcal{E}_4(\mathrm{zp})+\sum_{\sigma=1}^{3}\omega_{4\sigma}\Theta^{\dagger}_{4\sigma}\Theta_{4\sigma}+\tfrac{1}{2}\hat{N}^{(1)2}/M_4, \tag{2.50}$$

where M_4 is the pairing-rotational inertial parameter. The vibrational normal-mode boson creation operators corresponding to the frequency $\omega_{4\sigma}$ have the form:

$$\Theta^{\dagger}_{4\sigma}=X_{13}(4\sigma)B^{\dagger}_{13}+Y_{13}(4\sigma)B_{13}+X_{14}(4\sigma)B^{\dagger}_{14}+Y_{14}(4\sigma)B_{14}+X_{23}(4\sigma)B^{\dagger}_{23}+Y_{23}(4\sigma)B_{23}+X_{24}(4\sigma)B^{\dagger}_{24}+Y_{24}(4\sigma)B_{24} \tag{2.51}$$

and the total zero-point energy is $\mathcal{E}_4(\mathrm{zp})$.

If $\Delta=0$, there is no pairing rotation, but instead there are pairing vibrations. H_4 then takes the form

$$H_4=\mathcal{E}_4(\mathrm{zp})+\sum_{\sigma=1}^{4}\omega_{4\sigma}\Theta^{\dagger}_{4\sigma}\Theta_{4\sigma}. \tag{2.52}$$

Letting $\sigma=3,4$ denote the pairing vibrations, one finds that $\omega_{43}=\omega_{44}$, corresponding to a degeneracy of the two-particle and two-hole transfer modes.

The total yrast energy is the sum of the crank-

ing energy and the RPA zero-point energy:

$$\mathcal{E} = \mathcal{E}_0(\omega) + \mathcal{E}_3(\mathrm{zp}) + \mathcal{E}_4(\mathrm{zp}). \tag{2.53}$$

Both zero-point contributions provide corrections to the cranking model of the order Ω^{-1}, but $\mathcal{E}_3(\mathrm{zp})$ also provides corrections of the order of I^{-1}. It is important to note that in this way, the RPA improves the low-spin behavior of SCC1. Thus, at low spin, $\mathcal{E}_0$ goes as $\frac{1}{2}\mathcal{I}_0^{-1}I^2$, where $\mathcal{I}_0 = a^{-1} + \lim_{\omega\to 0}\langle j_x\rangle_\omega/\omega$. It is readily checked that $\mathcal{E}_4(\mathrm{zp})$ provides a correction $\frac{1}{2}\mathcal{I}_0^{-1}I$ to give the proper $I(I+1)$ dependence. It therefore follows that SCC2 must not be used with the RPA, since this correction would then be counted twice.

The special case when $\epsilon = 0$ is a very interesting limit, for one finds that SCC1 + RPA is then exact. In this limit, the "phase transition" is completely discontinuous. The $\Delta \neq 0$ solution as obtained from the gap equation (2.24) is just $\Delta = 2G\Omega$, for $\omega < 2G\Omega$, while $\Delta = 0$ for $\omega > 2G\Omega$. Making use of the results in the Appendix, the total energy (2.53) for $\Delta \neq 0$ is found to be

$$\mathcal{E} = \tfrac{1}{2}aI(I+1) - G\Omega(\Omega+1), \tag{2.54}$$

in complete agreement with the energy of the fully paired band as given in Ref. 8. The cranking model contributes $\frac{1}{2}aI^2 - G\Omega^2$ while the correction $\frac{1}{2}aI$, of relative order I^{-1}, is just $\mathcal{E}_3(\mathrm{zp})$, and the correction $-G\Omega$, of relative order Ω^{-1}, is $\mathcal{E}_4(\mathrm{zp})$. For $\Delta = 0$, one obtains

$$\mathcal{E} = \tfrac{1}{2}a(I-2\Omega)(I-2\Omega+1), \tag{2.55}$$

in complete agreement with the energy of the fully aligned band as given in Ref. 8. The cranking model contributes $\frac{1}{2}a(I-2\Omega)^2$ and $\mathcal{E}_3(\mathrm{zp}) = \frac{1}{2}a(I-2\Omega)$. $\mathcal{E}_4(\mathrm{zp})$ vanishes in this case.

Let us now consider the renormalization of the rotational frequency in the RPA. One begins with the usual relations $\omega_{\mathrm{RPA}} = d\mathcal{E}/d[I(I+1)]^{1/2}$ and $\mathcal{I}_{\mathrm{RPA}} = I[(I+1)]^{1/2}/\omega_{\mathrm{RPA}}$. However, it should be kept in mind that the energy $\mathcal{E}$ omits corrections of relative order I^{-1} (higher RPA corrections), so that for consistency the above definitions should be expanded in I^{-1}. One then finds that

$$\omega_{\mathrm{RPA}} = \omega + \delta\omega, \tag{2.56}$$

where ω is the cranking frequency and $\delta\omega$ is

$$\delta\omega = d[\mathcal{E}_3(\mathrm{zp}) + \mathcal{E}_4(\mathrm{zp})]/dI\,. \tag{2.57}$$

The moment of inertia $\mathcal{I}_{\mathrm{RPA}}$ to this order becomes

$$\mathcal{I}_{\mathrm{RPA}} = \mathcal{I}\left(1 - \frac{\delta\omega}{\omega} + \frac{1}{2I}\right), \tag{2.58}$$

where $\mathcal{I}$ is the SCC1 moment of inertia.

As a final point in this section, we call attention to the fact that H_3 and H_4 are not necessarily positive quadratic forms as is obvious from (2.36) and (2.39). Therefore, there is always the possibility of an onset of instability and the consequent breakdown of the cranking approximation. In particular, this can occur in the backbending region if the parameter a is sufficiently small. We return to this point later.

D. Variation after projection of particle number

Since self-consistent cranking, or any Hartree-Bogoliubov approximation, in general violates symmetries of the exact Hamiltonian, one may hope to improve the situation by projecting out from such wave functions the components with the correct symmetry. As noted previously, the R(8) model is not suitable for testing angular momentum projection, since the particle angular momentum is not a constant of motion of the exact Hamiltonian. On the other hand, particle number is conserved by H, but not by H_ω, and we may therefore apply particle-number projection, which has been used by several authors in the backbending region.[15] It is of interest to compare the projection method with the RPA, since both introduce correlations, and the RPA conserves particle number approximately (to order Ω^{-1}) through the pairing-rotation term.

For optimum results, the variation is performed after projection (VAPN). To improve the cranking model, the projected wave function ψ with particle number N, is given by

$$\psi = \mathfrak{N} P_N \Phi(\omega, \Delta), \tag{2.59}$$

where $\Phi(\omega, \Delta)$ is the ground state of H_ω (2.9), for arbitrary ω and Δ, $\mathfrak{N}$ is a normalization factor, and P_N is the usual projection operator to the subspace with N particles:

$$P_N = \frac{1}{2\pi i}\oint d\phi\, e^{i\phi(\hat{N}-N)}. \tag{2.60}$$

The parameters ω and Δ are then determined by the condition

$$\frac{\omega}{a} = [I(I+1)]^{1/2} - \langle\psi|j_x|\psi\rangle, \tag{2.61}$$

analogous to (2.14), and by the variational condition

$$\partial\mathcal{E}'_{\mathrm{proj}}(\omega, \Delta)/\partial\Delta = 0, \quad (\text{fixed } \omega), \tag{2.62}$$

where $\mathcal{E}'_{\mathrm{proj}}$ is defined by

$$\mathcal{E}'_{\mathrm{proj}} = \langle\psi|H_{\mathrm{s.p.}} - \omega j_x + H_p + H_j|\psi\rangle, \tag{2.63}$$

H_j being given by

$$H_j = \tfrac{1}{2}a(j_x^2 - \langle\psi|j_x|\psi\rangle^2 + j_y^2 + j_z^2). \tag{2.64}$$

The terms (2.64) are neglected in the cranking

model, but are taken into account by the RPA, and have therefore been included in (2.63) in order to provide a more valid comparison of VAPN and SCC1 + RPA.

The actual energy is not $\mathcal{E}'_{\rm proj}$, but $\mathcal{E}_{\rm proj}$, given by

$$\mathcal{E}_{\rm proj} = \tfrac{1}{2}\frac{\omega^2}{a} + \mathcal{E}'_{\rm proj} + \omega\langle\psi|j_x|\psi\rangle . \tag{2.65}$$

We note that if ψ is replaced by the unprojected Hartree-Bogoliubov state and the usual factorization of the interaction terms is used, then the above procedure reduces to self-consistent cranking.

The stationary points of $\mathcal{E}'_{\rm proj}$ are found numerically as a function of Δ for fixed ω. $\mathcal{E}'_{\rm proj}$ is evaluated using the method of "residuum integrals" first proposed by Dietrich, Mang, and Pradal.[16] This method is applicable when projecting from a wave function having the BCS *form*

$$\Phi = \prod_{\mu>0} (U_\mu + V_\mu c^\dagger_\mu c^\dagger_{\bar\mu})|0\rangle , \tag{2.66}$$

where $c^\dagger_\mu, c^\dagger_{\bar\mu}$ are fermion creation operators, with vacuum $|0\rangle$, and U_μ, V_μ are occupation amplitudes satisfying $U_\mu{}^2 + V_\mu{}^2 = 1$. The vacuum of H_ω has exactly this form, but the single-particle basis $|\mu\rangle = c^\dagger_\mu|0\rangle$ is the basis in which the one-particle density matrix and pairing tensor are in the "canonical form." The canonical basis is related to the $a^\dagger_\nu, b^\dagger_\nu$ basis by a unitary transformation. The states $c^\dagger_\mu, c^\dagger_{\bar\mu}$ which are paired in (2.66) are not time-reverse conjugate states since the term ωj_x violates time-reversal invariance. The pairing is defined dynamically by the canonical form. The method of Ref. 16, however, depends only on the form (2.66) and not on pairing of time-reverse conjugate states. Further details on the calculation of expectation values of one and two-body operators may be found in Ref. 16.

It can be shown that in the limit $\epsilon = 0$, VAPN reproduces the exact energies, as is the case for SCC1 + RPA.

III. $E2$ MATRIX ELEMENTS WITH SCC1 + RPA

In this section, the calculation of quadrupole matrix elements within the framework of SCC1 + RPA is illustrated. Although the R(8) model serves as a paradigm, the technique is obviously applicable to more realistic models, and since it is somewhat novel, it seems worthwhile to go into some detail.

The electric quadrupole operators have the form

$$\mathfrak{M}(E2,M) = \sum_K D^2_{MK}\mathfrak{M}'(E2,K) = \sum_K \hat D^2_{MK}\hat{\mathfrak{M}}'(E2,K), \tag{3.1}$$

where the operators D^2_{MK} are usually realized as representation matrix elements of the three-dimensional rotation group, and the $\mathfrak{M}'(E2,K)$ are intrinsic quadrupole operators. The $\hat D^2_{MK}$ and $\hat{\mathfrak{M}}'(E2,K)$ are the corresponding operators, but defined relative to quantization along the x axis in accord with the classical direction of the angular momentum. Following Krumlinde and Szymański, we write

$$\mathfrak{M}'(E2,K) = Q_c\,\delta_{K0} + \eta Q_{2K} , \tag{3.2}$$

where Q_c is the core quadrupole moment, Q_{2K} are the particle quadrupole operators, and η is a parameter. The Q_{2K} have been constructed in Ref. 8.[17] One can then write

$$\hat{\mathfrak{M}}'(E2,K) = Q^c_{2K} + \eta\hat Q_{2K} , \tag{3.3}$$

where the core contribution is given by

$$Q^c_{20} = -\tfrac{1}{2}Q_c , \quad Q^c_{2\pm1} = 0 , \quad Q^c_{2\pm2} = -\tfrac{1}{2}\sqrt{\tfrac{3}{2}}\,Q_c . \tag{3.4}$$

The particle operators, which satisfy the commutation rules

$$\begin{aligned} &[j_x, \hat Q_{2K}] = K\hat Q_{2K} , \\ &[j_y \pm i j_z, \hat Q_{2K}] = [6 - K(K\pm1)]^{1/2}\hat Q_{2K\pm1} , \end{aligned} \tag{3.5}$$

can be easily constructed as linear combinations of the Q_{2K}.

The next task is to transcribe the operators into the boson representation. First, consider the transcription of the core operators. Equations (2.32) express the total angular momentum operators projected on the intrinsic frame as functions of bosons $b, b^\dagger$. These relations can be interpreted as the leading order of a Holstein-Primakoff representation given by

$$\begin{aligned} I_x &= \hat I - b^\dagger b , \\ I_+ &= b^\dagger(2\hat I - b^\dagger b)^{1/2} , \\ I_- &= I_+^\dagger . \end{aligned} \tag{3.6}$$

At high spin, these operators can be defined on a space of functions

$$|IK\rangle = \frac{e^{iI\Phi}(b^\dagger)^{I-K}}{[2\pi(I-K)!\,]^{1/2}}|0\rangle , \tag{3.7}$$

where $|0\rangle$ is the boson vacuum, and then

$$\hat I = -i\frac{d}{d\Phi} . \tag{3.8}$$

As shown in Ref. 12, the states $|IK\rangle$ may be interpreted as a representation of the rotor eigenfunctions $|IMK\rangle$ having $M = I$, and then $\Phi = \phi + \psi$, the sum of two Euler angles. The bosons replace the θ degree of freedom.

Correspondingly, the core operators $\hat D^2_{MK}$ may be realized as functions of b, $b^\dagger$, and Φ, which

can be obtained from the commutation rules

$$[I_x, \hat{D}^2_{MK}] = K\hat{D}^2_{MK},$$
$$[I_\pm, \hat{D}^2_{MK}] = [6 - K(K \mp 1)]^{1/2}\hat{D}^2_{MK\mp 1}, \tag{3.9}$$

and the unitarity condition

$$\sum_K \hat{D}^{2\dagger}_{MK}\hat{D}^2_{M'K} = \delta_{MM'}. \tag{3.10}$$

For the RPA, one only requires the linear boson approximation, and the result is

$$\begin{aligned}
&\hat{D}^2_{00} = 1, \quad \hat{D}^2_{0-1} = (3/I)^{1/2}b^\dagger,\\
&\hat{D}^2_{-10} = -(3/I)^{1/2}e^{-i\Phi}b, \quad \hat{D}^2_{-1-1} = e^{-i\Phi},\\
&\hat{D}^2_{-1-2} = (2/I)^{1/2}e^{-i\Phi}b^\dagger,\\
&\hat{D}^2_{-2-1} = -(2/I)^{1/2}e^{-i2\Phi}b, \quad \hat{D}^2_{-2-2} = e^{-i2\Phi},
\end{aligned} \tag{3.11}$$

with all other $\hat{D}^2_{MK}$ with $M \leq 0$ vanishing in the RPA order. The $\hat{D}^2_{MK}$ with $M > 0$ can be obtained from the relation

$$\hat{D}^2_{-M-K} = (-)^{M-K}\hat{D}^{2\dagger}_{MK}. \tag{3.12}$$

Closed forms to all orders are given in Ref. 12.

The linear boson approximation to the intrinsic quadrupole operators is

$$\begin{aligned}
\hat{Q}_{20} \approx{}& \langle \hat{Q}_{20}\rangle_\omega + q^{(0)}_{13}(B^\dagger_{13} + B_{13}) + q^{(0)}_{24}(B^\dagger_{24} + B_{24})\\
&+ q^{(0)}_{14}(B^\dagger_{14} + B_{14} - B^\dagger_{23} - B_{23}),
\end{aligned} \tag{3.13a}$$

$$\hat{Q}_{21} \approx q^{(1)}_{12}(B^\dagger_{12} + B_{34}), \quad \hat{Q}_{2-1} = -\hat{Q}^\dagger_{21}, \tag{3.13b}$$

$$\begin{aligned}
\hat{Q}_{22} \approx{}& \langle \hat{Q}_{22}\rangle_\omega + q^{(2)}_{13}B^\dagger_{13} + p^{(2)}_{13}B_{13} + q^{(2)}_{24}B^\dagger_{24}\\
&+ p^{(2)}_{24}B_{24}, \quad \hat{Q}_{2-2} = \hat{Q}^\dagger_{22}.
\end{aligned} \tag{3.13c}$$

The expectation values with respect to the vacuum of H_ω, $\langle \hat{Q}_{20}\rangle_\omega$ and $\langle \hat{Q}_{22}\rangle_\omega$, are given by

$$\langle \hat{Q}_{20}\rangle_\omega = \frac{\epsilon(E_+ - E_-)[(E_+ + E_-)^2 - 4\omega^2]}{(8\gamma E_+ E_-\omega)}, \tag{3.14a}$$

$$\langle \hat{Q}_{22}\rangle_\omega = \frac{1}{4}\left(\frac{3}{2}\right)^{1/2}\frac{\epsilon\Omega}{E_+E_-}(E_+ + E_-). \tag{3.14b}$$

The remaining coefficients are explicitly as follows:

$$\begin{aligned}
&q^{(0)}_{13} = (3\Omega)^{1/2}\epsilon^2/(4\gamma E_-), \quad q^{(0)}_{24} = (3\Omega)^{1/2}\epsilon^2/(4\gamma E_+),\\
&q^{(0)}_{14} = -q^{(0)}_{23} = -\frac{2\Delta}{\gamma}\left[\frac{\Omega(E_+ + E_-)}{8G}\right]^{1/2},\\
&q^{(1)}_{12} = \left[\frac{\gamma\Omega(E_+ + E_-)}{8}\left(\frac{\gamma + 2\omega}{E_+} + \frac{\gamma - 2\omega}{E_-}\right)\right]^{1/2},\\
&q^{(2)}_{13} = -\left(\frac{\Omega}{32}\right)^{1/2}\left(\frac{\gamma - 2\omega}{E_-} + 2\right),\\
&p^{(2)}_{13} = -\left(\frac{\Omega}{32}\right)^{1/2}\left(\frac{\gamma - 2\omega}{E_-} - 2\right),\\
&q^{(2)}_{24} = -\left(\frac{\Omega}{32}\right)^{1/2}\left(\frac{\gamma + 2\omega}{E_+} - 2\right),\\
&p^{(2)}_{24} = -\left(\frac{\Omega}{32}\right)^{1/2}\left(\frac{\gamma + 2\omega}{E_+} + 2\right).
\end{aligned} \tag{3.15}$$

From (3.1)–(3.5), (3.11), and (3.13), the electric quadrupole operators in the RPA order are given by

$$\begin{aligned}
&\mathfrak{M}(E2, 0) \approx -\tfrac{1}{2}Q_c + \eta\hat{Q}_{20},\\
&\mathfrak{M}(E2, -2) \approx e^{-i2\Phi}(-\tfrac{1}{2}\sqrt{\tfrac{3}{2}}Q_c + \eta\hat{Q}_{2-2}),\\
&\mathfrak{M}(E2, -1) \approx e^{-i\Phi}\{\tfrac{1}{2}Q_c(3/I)^{1/2}(b - b^\dagger)\\
&\qquad + \eta[-(3/I)^{1/2}\langle \hat{Q}_{20}\rangle_\omega b + (2/I)^{1/2}\\
&\qquad \times \langle \hat{Q}_{22}\rangle_\omega b^\dagger - q^{(1)}_{12}(B^\dagger_{34} + B_{12})]\},
\end{aligned} \tag{3.16}$$

where $\hat{Q}_{20}$ and $\hat{Q}_{2-2}$ are given by (3.13). The next step, of course, is to express (3.16) in terms of the normal-mode bosons. In the following, we ignore $\mathfrak{M}(E2, -1)$ which is responsible for $\Delta I = 1$ transitions. The other transition operators have the form

$$\begin{aligned}
&\mathfrak{M}(E2, 0) = -\tfrac{1}{2}Q_c + \eta\langle \hat{Q}_{20}\rangle_\omega + \eta\sum_\sigma\sum_{i>j} q^{(\omega)}_{ij}[X_{ij}(4\sigma) - Y_{ij}(4\sigma)](\mathcal{O}^\dagger_{4\sigma} + \mathcal{O}_{4\sigma}),\\
&\mathfrak{M}(E2, -2) = e^{-i2\Phi}(-\tfrac{1}{2}\sqrt{\tfrac{3}{2}}Q_c + \eta\langle \hat{Q}_{22}\rangle_\omega) + e^{-i2\Phi}\eta\sum_\sigma\sum_{i>j}\{[p^{(2)}_{ij}X_{ij}(4\sigma) - q^{(2)}_{ij}Y_{ij}(4\sigma)]\mathcal{O}^\dagger_{4\sigma}\\
&\qquad + [q^{(2)}_{ij}X_{ij}(4\sigma) - p^{(2)}_{ij}Y_{ij}(4\sigma)]\mathcal{O}_{4\sigma}\}.
\end{aligned} \tag{3.17}$$

The first two constant terms of $\mathfrak{M}(E2, 0)$ give the static electric quadrupole moment of the yrast band, while the second term is responsible for $\Delta I = 0$ transitions involving a change of one phonon. The operator $\mathfrak{M}(E2, -2)$ is responsible for $I \to I - 2$ transitions. The first term accounts for the stretched $E2$ transitions along the yrast cascade, while the second accounts for transitions involving a change of one phonon. The $B(E2)$'s involving a change in the number of phonons are weaker by a factor of the order of Ω^{-1} (the order of the RPA amplitudes squared) compared to the yrast cas-

cade, which is just the type of selection rule required to account for the experimental data.

The $\Delta I = 2$ matrix elements require some additional discussion. In general, these have the form

$$\langle n' I' \omega(I') | \mathfrak{M}(E2, -2) | n I \omega(I) \rangle ,$$

where n collectively denotes the phonon numbers, I the total angular momentum, and $\omega(I)$ the cranking-model angular velocity as a function of I. Since the rotor wave functions (3.7) have a factor $(2\pi)^{-1/2} e^{iI\Phi}$, this factor occurs in the wave function $|nI\omega\rangle$. We therefore see that states having different values of I are automatically orthogonal. The operator $\mathfrak{M}(E2, -2)$ decreases I by two units in the exponential. However $\omega(I-2) \neq \omega(I)$ so that the underlying cranking-model states are different. For example, the transition matrix element along the yrast line is given by

$$\langle n=0\, I-2\, \omega(I-2) | \mathfrak{M}(E2,-2) | n=0\, I\, \omega(I) \rangle = (-\tfrac{1}{2}\sqrt{\tfrac{3}{2}} Q_c + \eta \langle \hat{Q}_{22} \rangle_\omega)\, {}_{\mathrm{RPA}}\langle \omega(I-2) | \omega(I) \rangle_{\mathrm{RPA}} + \eta \sum_\sigma \sum_{i>j} [p^{(2)}_{ij} X_{ij}(4\sigma) - q^{(2)}_{ij} Y_{ij}(4\sigma)]\, {}_{\mathrm{RPA}}\langle \omega(I-2) | \mathcal{O}^\dagger_{4\sigma} | \omega(I) \rangle_{\mathrm{RPA}} + \cdots , \tag{3.18}$$

where $|\omega(I)\rangle_{\mathrm{RPA}}$ is the vacuum corresponding to a cranking solution with frequency $\omega(I)$. The states $|\omega(I)\rangle_{\mathrm{RPA}}$ and $|\omega(I-2)\rangle_{\mathrm{RPA}}$ are not orthogonal. Also, we have that although $\mathcal{O}_{4\sigma} |\omega(I)\rangle_{\mathrm{RPA}} = 0$, ${}_{\mathrm{RPA}}\langle \omega(I-2) | \mathcal{O}^\dagger_{4\sigma} \neq 0$. In general, then, one must calculate overlap integrals, and not simply between Hartree-Bogoliubov states, but between the corresponding RPA vacuum states, which is still more difficult. However, if I is sufficiently large and outside of the neighborhood of the phase transition, one may assume

$$|\omega(I-2)\rangle_{\mathrm{RPA}} \approx |\omega(I)\rangle_{\mathrm{RPA}} . \tag{3.19}$$

Then (3.18) simplifies to

$$\langle n=0\, I-2\, \omega(I-2) | \mathfrak{M}(E2,-2) | n=0\, I\, \omega(I) \rangle \approx -\tfrac{1}{2}\sqrt{\tfrac{3}{2}} Q_c + \eta \langle \hat{Q}_{22} \rangle_\omega , \tag{3.20}$$

which is determined by the SCC expectation value $\langle \hat{Q}_{22} \rangle_\omega$. The approximation (3.19) is fully consistent with the expansion in powers of I^{-1} which led us to (3.17).

In the neighborhood of the phase transition, however, the two vacuum states may have radically different character—$|\omega(I-2)\rangle_{\mathrm{RPA}}$ may correspond to an essentially paired state and $|\omega(I)\rangle_{\mathrm{RPA}}$ to the aligned state. In that case, the approximation (3.19) can be expected to break down. It may still be a good approximation to simply multiply (3.20) by the overlap ${}_{\mathrm{RPA}}\langle \omega(I-2) | \omega(I) \rangle_{\mathrm{RPA}}$, but such a calculation is beyond the scope of this paper.

The static quadrupole moment along the yrast line is given by

$$\langle n=0\, I\, \omega | \mathfrak{M}(E2,0) | n=0\, I\, \omega \rangle = -\tfrac{1}{2} Q_c + \eta \langle \hat{Q}_{20} \rangle_\omega . \tag{3.21}$$

Here, there is no problem with overlap integrals and everything is determined by the cranking model.

IV. NUMERICAL CALCULATIONS

A. Choice of parameters

Because of the size of the matrices to be diagonalized, the maximum value of Ω for which exact solutions could be practicably obtained with our computing facilities was $\Omega = 4$.[18] This means we were limited to not more than eight particles, a number significantly smaller than that occurring in realistic calculations. Since the many-body methods against which the exact solutions are to be compared become more accurate as Ω increases, we cannot display these methods in the most favorable light. Just for this reason, one is all the more impressed by the favorable comparison which emerges.

The degree of backbending is controlled mainly by the ratio $\epsilon/(G\Omega)$: the smaller the ratio, the weaker the band mixing and the greater the tendency to bend back. We have followed the procedure of keeping G fixed and varying ϵ to control the degree of backbending. Exact solutions were obtained for $\Omega = 3$, $G = 0.1$, $a = 0.02$, and $\epsilon = 0.05$, 0.10, 0.15, and 0.20, and $\Omega = 4$, $G = 0.075$, $a = 0.019\,736$, and $\epsilon = 0.05$, 0.10, and 0.15, which covers the range from sharp backbending to no backbending and a smooth transition.

As shown in Ref. 8, the critical angular momentum I_c is given by

$$I_c = \Omega - \tfrac{1}{2} + \tfrac{1}{2}(G/a)(\Omega+1) . \tag{4.1}$$

The ratio G/a was fixed by the requirement that the phase transition occur between $I = 12$–14, in rough accord with experiment. The values of G were arbitrarily chosen to maintain about the same magnitude of ground-state pair correlations as in Ref. 8.

The salient features emerging from the calcula-

tions are summarized in some representative figures and tables.

B. Results of calculations

1. Regions of stability and instability

It is seen from the figures that the yrast trajectories can have several regions of interest. The simplest picture is provided by the cranking model, in which the trajectories are composed of two segments, one with $\Delta \neq 0$, which may or may not have a backbending region (depending on the value of $\epsilon/G\Omega$), along which Δ decreases and $\mathcal{I}$ increases continuously with increasing ω^2 until the intersection with the $\Delta = 0$ segment at some $\omega = \omega^*$, corresponding to a cusp. For $\omega^2 < \omega^{*2}$, the $\Delta = 0$ solution is unstable and is omitted. The situation becomes more complicated after adding the corrections due to the RPA, which tests the stability of the self-consistent cranking solutions.

The $\Delta = 0$ segment is always stable for $\omega^2 > \omega^{*2}$, but as $\omega \to \omega^*$, the doubly degenerate pairing vibration [(A35)] drops to zero frequency, signaling the onset of the transition from a pair-vibrational to a pair-rotational scheme. As ω^* is approached along the $\Delta \neq 0$ segment, one of the RPA frequencies approaches zero, in addition to the already present zero-frequency solution corresponding to the pair rotation. Also, as ω^* is approached along either segment, $d\mathcal{E}(\mathrm{zp})/dI$, the derivative of the zero-point energy with respect to angular momentum, becomes infinite and therefore so does $\delta\omega$ defined by (2.57). Therefore, the RPA correction breaks down completely at the cusp, accounting for the hiatus in the RPA curves.

The $\Delta \neq 0$ segment can show instabilities since the RPA quadratic form is not necessarily positive. In our calculations, instability was indicated by an eigenfrequency of H_4 passing through zero and turning imaginary. An unstable region occurs only along a portion of a backbending part, and only if the parameter a is sufficiently small compared to $G\Omega/\epsilon$. That is, the rotor must be sufficiently massive and the pairing correlations sufficiently strong. The unstable region is indicated by a dotted line in the figures. Figure 1, for example, shows quite clearly that as ϵ is increased for fixed a and $G\Omega$, the unstable region decreases in size. This instability in the backbending region is the result of competition between the particles, which favor increasing I with decreasing $|\omega|$ (the effect is proportional to $G\Omega/\epsilon$), and the rotor, which favors decreasing I with decreasing $|\omega|$ (the effect is proportional to a^{-1}). Figure 2, which is a plot of I vs $|\omega|$, shows that in the unstable region the rotor wins out, producing the peculiar "down bending." This is to be contrasted with Fig. 3, with another set of parameters, such that the yrast trajectories are stable everywhere. In this case, I increases with decreasing angular velocity in the backbending region. Fortunately, in realistic calculations an external rotor introduced to simulate a core would normally be small enough to avoid instability problems of this kind. In fact, in an ideal calculation utilizing a rotationally invariant particle Hamiltonian and a sufficiently large single-

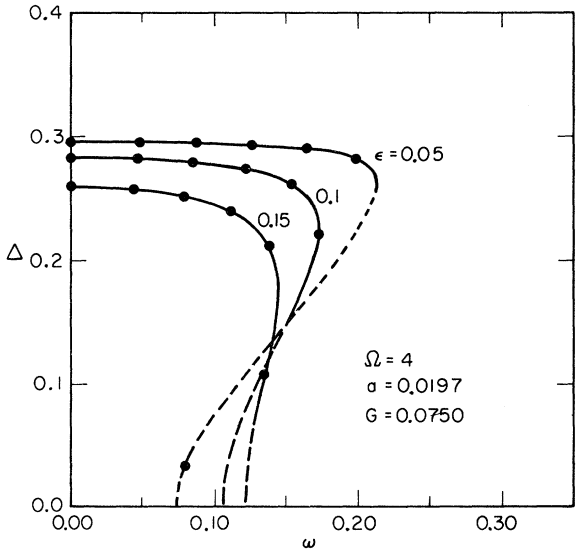

FIG. 1. The gap parameter Δ as a function of angular speed ω for SCC2. The discrete points correspond to integer values of angular momentum. The cranking-model solutions are unstable along the dashed portions of the curves.

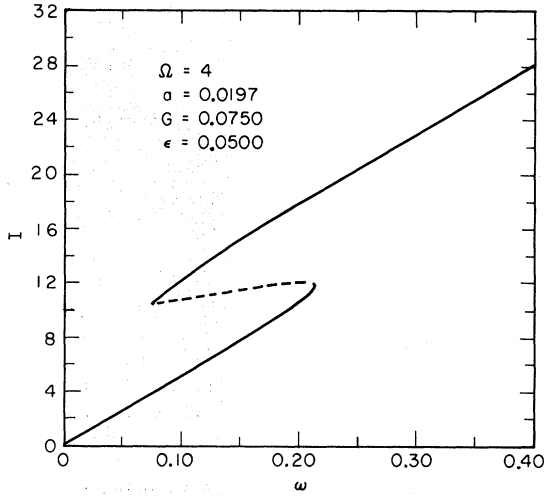

FIG. 2. The spin I as a function of angular speed ω for SCC2. The cranking-model solution is unstable along the dashed part of the curve.

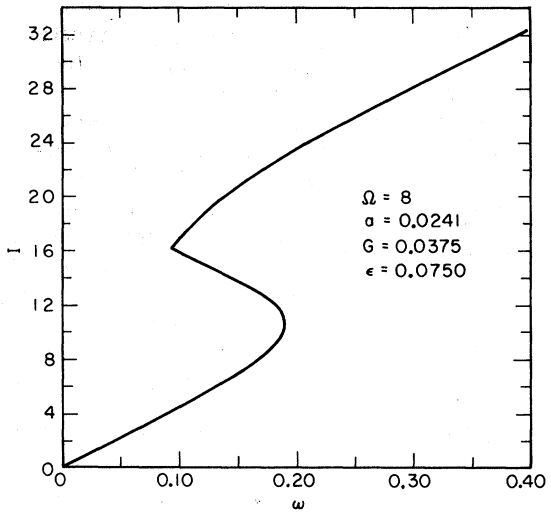

FIG. 3. The spin I as a function of angular speed ω for SCC2. The cranking-model solution is stable everywhere.

particle space no rotor need be introduced.

It has been seen that backbending per se does not necessarily imply instability (the criterion for which is the existence of an imaginary RPA frequency) as illustrated by Fig. 3. This is a counterexample to some claims made in previous work.[19] It is easy to see how one can be easily misled on this point by considering a contour map of the cranking energy $\mathcal{E}_0'(\omega, \Delta)$ defined by

$$\mathcal{E}_0'(\omega, \Delta) = \mathcal{E}_0(\omega, \Delta) - \omega[\langle j_x \rangle_\omega + \omega/a]. \tag{4.2}$$

The quantity in square brackets is the total angular momentum [(2.25)], and $\mathcal{E}_0(\omega, \Delta)$ is given by

$$\mathcal{E}_0(\omega, \Delta) = \tfrac{1}{2}\omega^2/a + \langle H_{\text{s.p.}} \rangle - G\left[\frac{\Delta\Omega}{2\gamma}\left(\frac{\gamma + 2\omega}{E_+} + \frac{\gamma - 2\omega}{E_-}\right)\right]^2, \tag{4.3}$$

which reduces to (2.10) at self-consistency. It is clear that (4.2) is independent of whether SCC1 or SCC2 is chosen.

Actually, Fig. 4 is a plot of $\mathcal{E}_0'(\omega, \Delta) + \omega^2/a$, which is topologically equivalent to $\mathcal{E}_0'$, but shows the interesting features more clearly than the latter. We see from the plot that the self-consistent solution along the backbending region corresponds to a *maximum* in $\mathcal{E}_0'$ as a function of Δ for fixed ω. The nonbackbending regions, on the other hand, do correspond to a minimum. This illustrates in essence the basis of the claim that the backbending region corresponds to an unstable self-consistent cranking solution.

In fact, however, the apparent instability is a misleading artefact resulting from (i), using $\mathcal{E}_0'$ rather than $\mathcal{E}_0$, and (ii), using variations for fixed angular velocity rather than fixed angular momentum. Similar situations have been recognized in the classical theory of rotating fluids.[20] To properly assess the stability one should study variations of the energy $\mathcal{E}_0$, relative to the laboratory frame, for fixed I. Figure 5 is a contour plot of $\mathcal{E}_0(I, \Delta)$ which shows that the instability in fact disappears. It can be shown that the correct stability criterion is in accord with the RPA criterion as used in the

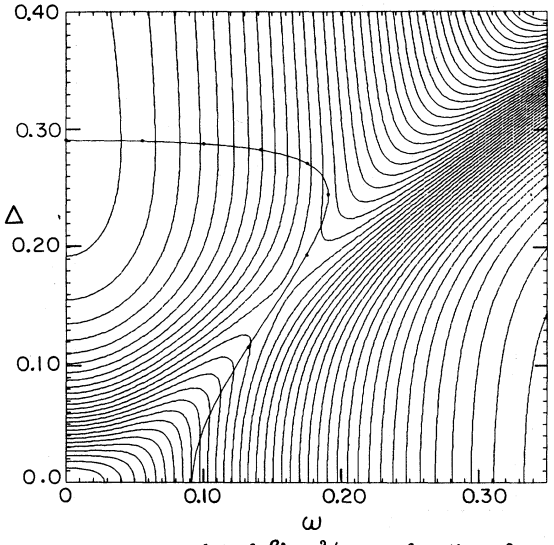

FIG. 4. Contour plot of $\mathcal{E}_0' + \omega^2/a$ as a function of ω and Δ (SCC2). The self-consistent solution $\Delta(\omega)$ is given by the backbending curve with discrete points which correspond to integer spins. Parameters are the same as in Fig. 3.

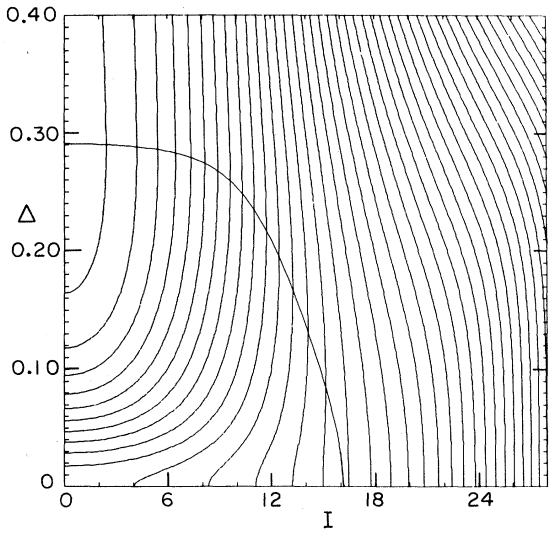

FIG. 5. Contour plot of the SCC2 energy $\mathcal{E}_0$ as a function of ω and I. The self-consistent solution $\Delta(I)$ is the locus of points corresponding to the minimum of $\mathcal{E}_0(I, \Delta)$ for fixed I. Parameters are the same as in Fig. 3.

TABLE I. Yrast energies. The cranking energy $\mathcal{E}_0$ corresponds to SCC1. The RPA zero-point corrections $\mathcal{E}_3(\mathrm{zp})$ and $\mathcal{E}_4(\mathrm{zp})$ are listed separately, together with the contribution to each of the zero-frequency modes. Column 7 lists the sum $\mathcal{E}_0+\mathcal{E}_3(\mathrm{zp})+\mathcal{E}_4(\mathrm{zp})$. Column 8 lists the projected energies $\mathcal{E}_{\mathrm{proj}}$ and the last column the exact energies.

		$\mathcal{E}_3(\mathrm{zp})$		$\mathcal{E}_4(\mathrm{zp})$				
I	SCC1	Zero mode	Total	Zero mode	Total	SCC1+RPA	Projected	Exact
0	−1.3333	−0.0000	0.0065	−0.1500	−0.3107	−1.6375	−1.6392	−1.6399
2	−1.2955	−0.0004	0.0255	−0.1498	−0.3106	−1.5806	−1.5822	−1.5830
4	−1.1825	−0.0009	0.0445	−0.1491	−0.3102	−1.4482	−1.4496	−1.4507
6	−0.9956	−0.0017	0.0635	−0.1475	−0.3093	−1.2414	−1.2424	−1.2443
8	−0.7380	−0.0029	0.0818	−0.1440	−0.3069	−0.9632	−0.9633	−0.9669
10	−0.4192	−0.0058	0.0974	−0.1338	−0.2992	−0.6209	−0.6183	−0.6266
12	−0.1332	−0.0291	0.0842	0	−0.1410	−0.1900	−0.2304	−0.2506
14	−0.1297	−0.0273	0.3518	0	−0.0827	0.1394	0.1527	0.1132
16	0.4516	−0.0233	0.1033	0	−0.0540	0.5009	0.5397	0.4884
18	0.8389	−0.0188	0.1167	0	−0.0374	0.9182	0.9705	0.9112
20	1.2961	−0.0147	0.1320	0	−0.0271	1.4010	1.4613	1.3968
22	1.8264	−0.0115	0.1486	0	−0.0204	1.9546	2.0200	1.9519
24	2.4316	−0.0090	0.1662	0	−0.0159	2.5819	2.6506	2.5800
26	3.1130	−0.0072	0.1843	0	−0.0127	3.2846	3.3557	3.2833
28	3.8713	−0.0058	0.2029	0	−0.0104	4.0638	4.1365	4.0628

present work.

For good measure, we emphasize that the spurious instability itself is not due to the cranking model, but is an inherent property of backbending. It would occur with any variational wave function, such as the particle-number projected wave function, or, for that matter, with an exact eigenstate of H. Although the stability aspects were discussed for the R(8) model, we believe the features hold for more general cases, but we have no general proofs at this time.

2. *Comparison of approximate and exact energies*

Since, as was already noted, the VAPN and the SCC1+RPA energies are both exact in the limit $\epsilon=0$, it is clear that these two methods will be superior for very small ϵ (very sharp backbending), except that the second method breaks down in a small neighborhood of the cusp. A more realistic comparison is provided by the intermediate case with $\Omega=4$, $\epsilon=0.1$, given in Table I, which also presents an enumeration of SCC1+RPA contributions. From this, one can see that the zero-

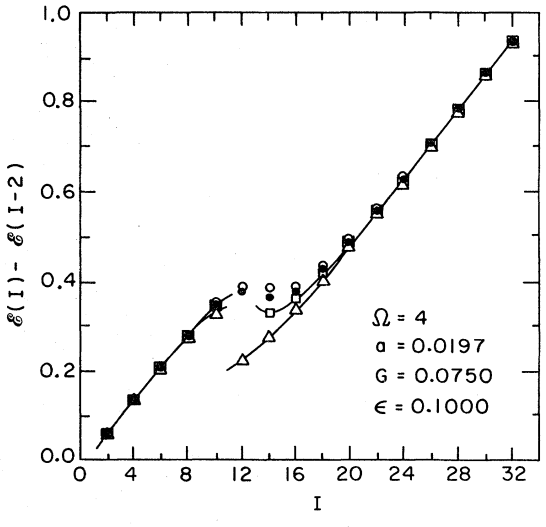

FIG. 6. Yrast excitation energies vs spin I. Symbols are as follows: ●, exact; △, SCC2; □, SCC1+RPA; ○, VAPN.

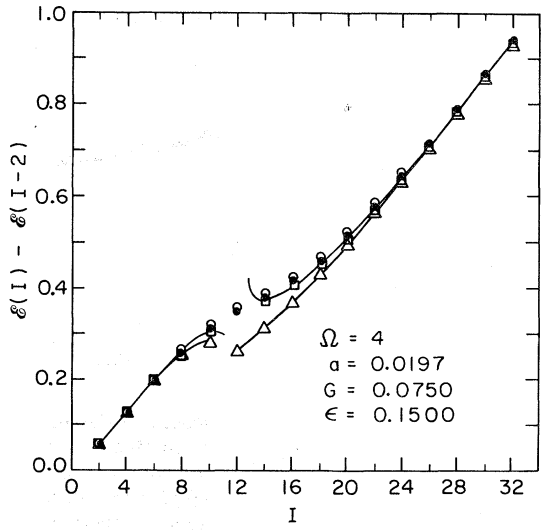

FIG. 7. Yrast excitation energies vs spin I. Symbols as the same as Fig. 6.

point contributions of the zero-frequency modes play a very important role. Figure 6 is a plot of the yrast excitation energies vs I for this case, while Fig. 7 is a similar plot for the case $\Omega = 4$, $\epsilon = 0.15$, in which the backbending disappears.

It is seen that all three methods, SCC2, SCC1 +RPA, and VAPN are pleasingly accurate on the upper and lower branches outside of the transition region. The least embellished method SCC2 is also least accurate, especially in the transition region, although it is asymptotically exact in the classical limit of large I, where all the methods eventually converge. The transition region, however, only encompasses three states or so. Clearly, SCC1 +RPA provides a nice improvement with only a bit more expenditure of time, except for the failure in the neighborhood of $I = 12$, due partly to the pernicious influence of the cusp and partly to the large amplitude of the pair fluctuations. These effects, however, present no problem for the VAPN method, which is quite good all the way through. It turns out to be very important to include the contribution (2.64) in the VAPN to achieve good results. For large I, the absolute energies given by SCC1 +RPA are better than those given by VAPN.

As ϵ increases so that the backbending disappears, the VAPN method emerges as the best. SCC is also significantly less accurate with no backbending than with sharp backbending, which

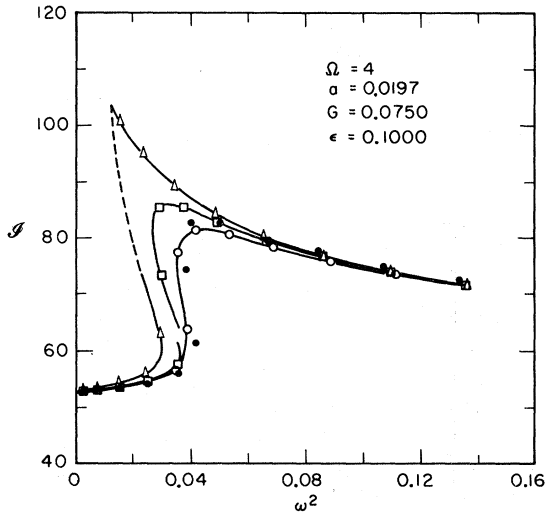

FIG. 8. Moment of inertia vs square of the angular speed. The theoretical values are obtained by differentiating the energy as a *continuous* function of spin. The "exact" values are obtained by applying the finite-difference formula to the exact energies as a function of integer values of spin. The dashed portion of the SCC2 curve is unstable. Symbols are the same as Fig. 6.

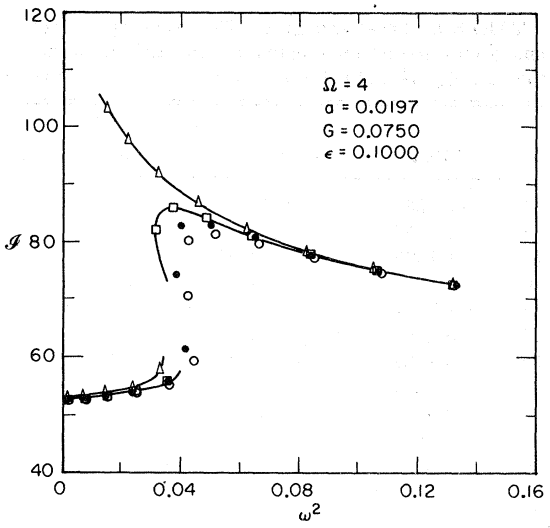

FIG. 9. Moment of inertia vs square of the angular speed. The finite difference formula is applied to both theoretical and exact energies as a function of integer values of spin. Symbols are the same as Fig. 6.

may be a general rule since this result is a consequence of the enlargement of the transition region in which the two bands are strongly mixed and zero-point oscillations become important.

The results may also be presented in the popular way as a plot of the moment of inertia vs angular speed. But then some ambiguity enters. In one type of plot, exemplified by Fig. 8, the "theoretical" values of $\mathcal{J}$ are plotted as continuous functions of the corresponding value of ω, while the "experimental" values are obtained from the finite

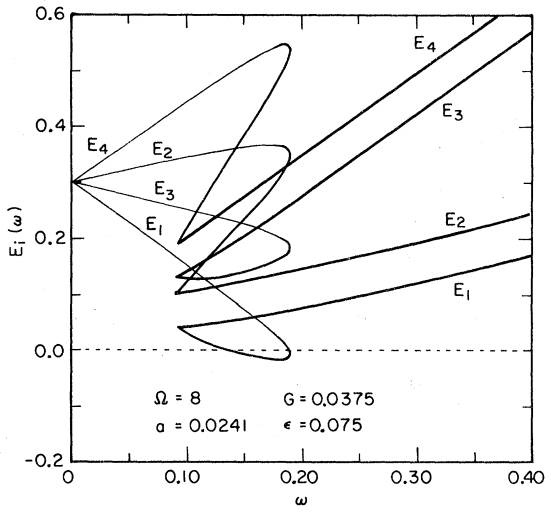

FIG. 10. The quasiparticle energies vs angular speed.

TABLE II. Static and transition quadrupole moments along the yrast line. The transition quadrupole moment is defined here as $[B(E2;I\to I-2)]^{1/2}$. The approximate values are defined by (3.21) and (3.20) and completely determined by SCC1. The exact values are defined in Ref. 8. In all cases, the choice of parameters is: $Q_c=0$, $\eta=1$, $\Omega=3$, $G=0.1$, and $a=0.02$. Results are given for different values of ϵ.

	$\epsilon=0.05$				$\epsilon=0.10$				$\epsilon=0.15$				$\epsilon=0.20$			
	Static		Transition		Static		Transition		Static		Transition		Static		Transition	
I	SCC1	Exact	SCC1	Exact	SCC1	Exact	SCC1	Exact	SCC1	Exact	SCC1	Exact	SCC1	Exact	SCC1	Exact
2	0.250	0.214	0.312	0.232	0.500	0.438	0.623	0.475	0.750	0.663	0.933	0.720	1.000	0.836	1.243	0.915
4	0.250	0.214	0.329	0.239	0.500	0.439	0.656	0.488	0.750	0.661	0.979	0.736	1.000	0.826	1.299	0.927
6	0.250	0.214	0.364	0.263	0.500	0.440	0.721	0.516	0.750	0.655	1.068	0.769	1.000	0.805	1.407	0.951
8	0.250	0.215	0.426	0.278	0.500	0.442	0.842	0.564	0.750	0.640	1.235	0.818	1.000	0.770	1.601	0.982
10	0.250	0.216	0.554	0.321	0.500	0.438	1.145	0.638	0.683	0.603	1.545	0.879	0.889	0.712	1.659	1.015
12	0.062	0.216	0.705	0.389	0.276	0.390	1.165	0.721	0.514	0.524	1.420	0.933	0.713	0.629	1.564	1.039
14	0.030	0.069	0.552	0.261	0.168	0.254	0.986	0.772	0.364	0.407	1.274	0.954	0.556	0.526	1.454	1.042
16	0.016	0.027	0.449	0.483	0.104	0.145	0.839	0.765	0.255	0.291	1.134	0.925	0.425	0.419	1.339	1.018
18	0.010	0.014	0.377	0.386	0.067	0.085	0.723	0.676	0.179	0.201	1.008	0.857	0.322	0.323	1.224	0.969
20	0.006	0.008	0.325	0.316	0.045	0.053	0.631	0.582	0.127	0.139	0.899	0.775	0.243	0.244	1.117	0.906
22	0.004	0.005	0.285	0.266	0.031	0.035	0.558	0.504	0.092	0.098	0.807	0.695	0.185	0.183	1.019	0.837
24	0.003	0.003	0.254	0.229	0.022	0.024	0.500	0.442	0.068	0.070	0.729	0.623	0.142	0.139	0.933	0.768
26	0.002	0.003	0.229	0.201	0.017	0.017	0.452	0.392	0.052	0.052	0.664	0.562	0.110	0.106	0.857	0.705
28	0.002	0.002	0.208	0.179	0.013	0.013	0.412	0.351	0.040	0.039	0.608	0.509	0.087	0.082	0.791	0.648

difference formulas

$$\omega^2 \approx 4(I^2-I+1)\left[\frac{\mathcal{E}(I)-\mathcal{E}(I-2)}{4I-2}\right]^2,$$
$$\mathcal{J}=\frac{1}{2}\left[\frac{\mathcal{E}(I)-\mathcal{E}(I-2)}{4I-2}\right]^{-1}. \tag{4.4}$$

In actuality, then, one is comparing somewhat different quantities. The alternative is to apply the formulas (4.4) to both the theoretical and experimental data. As can be seen from Fig. 9, the comparison is slightly better. The disadvantage is that one is presenting an approximation to the theoretical $\mathcal{J}$ vs ω curve when the full continuous curve is known. Perhaps the best way to avoid such problems is to simply plot the excitation energies vs angular momentum for all cases.

As a final point connected with energies, Fig. 10 is a plot of the quasiparticle energies defined by (2.17) as a self-consistent function of the angular velocity. The plot shows that the lowest quasiparticle energy E_1 can turn negative for certain values of ω, corresponding to gapless superconductivity. Moreover, the curve displays an intriguing knot when plotted in this way. The occurrence of this phenomenon is a function of the choice of parameters. We have found that backbending is strongly correlated with gapless superconductivity, as has been suggested elsewhere, but the correspondence is by no means one-one.[4] In particular, we have found instances of backbending concomitant with entirely positive values for all quasiparticle energies. This is no surprise, since the R(5) model exhibits backbending while completely excluding gapless superconductivity.

3. *Comparison of transition matrix elements*

Because of computing limitations, it was possible for us to calculate exact transition matrix elements only along the yrast line, and then only for cases with $\Omega=3$. Table II is a comparison of the exact and approximate matrix elements, corresponding to (3.20) and (3.21), with $\eta=1$ and $Q_c=0$. The approximate matrix elements are not as accurate as the corresponding energies. The breakdown of SCC in the transition region is clearly evident, but the transition quadrupole moment suffers more than the static quadrupole moment. This is just what was expected as a consequence of the neglected overlap integrals in the former case. The improvement of the approximate static moment with increasing I is clearly evident, and expected from the nature of the approximations. Considering the small number of particles (six), the comparison is really quite good. We expect that with the large number of particles in a realistic calculation, the cranking model should provide a reliable

and simple method for calculating static moments of the yrast band, outside of the transition region and for calculating the yrast cascade, which is a topic of great current interest.

V. SUMMARY

Of the three many-body methods tested on the R(8) model, SCC2, the most simple, is also least accurate. Nevertheless, it is still a very reasonable approximation except in the transition region, but this only encompasses two or three yrast states. In the classical limit, $I \to \infty$, SCC2 becomes exact. A significant improvement is provided by SCC1+RPA, which extends the usefulness of self-consistent cranking a little further into the transition region at little extra cost. However, the RPA correlations do break down over part of the transition region, owing mostly to the singularity at the cusp, but also in part to the large magnitude of the pair fluctuations. In realistic cases, it appears that the observed "phase transition" is due mainly to the complete alignment of a single pair of nucleons in high-j orbitals.[2] While the value of Δ is then attenuated, it does not vanish, so that the cusp does not occur in this region. Of course, at some higher value of $\omega = \omega^*$ for which additional nucleons align, the blocking effect will cause Δ to vanish and a cusp will occur. If the pair fluctuations are not too large, the validity of the RPA may extend beyond the phase transition to $\omega = \omega^*$, and then again for ω beyond this value.

The VAPN results are quite comparable to SCC1+RPA, except in the transition region. Since a discontinuity in Δ does not occur with projected wave functions, there is no problem with a cusp. Thus, the projected energies sail right through the transition region, although they are relatively less accurate there than elsewhere. The price one pays is additional difficulty in computation. In particular, realistic calculations of transition probabilities would require both angular-momentum and particle-number projection. The SCC1+RPA method, on the other hand, provides a simple prescription for calculating transition probabilities *at high spin*, not only along the yrast line, but also between excited states built on the yrast line. One can then calculate properties of the yrast cascade. The method can also be systematically improved by the boson-expansion technique.

Finally, it is perhaps worthwhile to point out that the exact, that is, group-theory based shell model calculation is of the order of 100 times slower than the approximate many-body methods. A comparison of the accuracy, to say nothing of physical insight, makes the appropriate choice of technique in this kind of situation clear-cut.

APPENDIX: DIAGONALIZATION OF H_{RPA}

The details of diagonalizing the quadratic forms defined by (2.35)–(2.42) are outlined below.

First consider H_3. The separation of the zero-energy mode, defined by (2.44), can be achieved by the method of Ref. 14. One seeks a variable Θ canonically conjugate to $(I_z - j_z)^{(1)}$,

$$[\Theta, (I_z - j_z)^{(1)}] = i\,, \tag{A1}$$

which commutes with the intrinsic bosons $\mathcal{O}_{3\sigma}, \mathcal{O}^\dagger_{3\sigma}$. Taking note of (2.46), Θ must satisfy the inhomogeneous equation

$$[H_3, \Theta] = -iM_3^{-1}(I_z - j_z)^{(1)}\,. \tag{A2}$$

From the form of $(I_z - j_z)^{(1)}$, it is obvious that Θ must have the form

$$\Theta = Z(b^\dagger + b) + Z_{12}(B^\dagger_{12} + B_{12}) + Z_{34}(B^\dagger_{34} + B_{34})\,. \tag{A3}$$

The coefficients of $M_3\Theta$ are obtained by solving (A2), while the inertial parameter M_3 is fixed by the normalization (A1). [It is somewhat easier to work with $H_3' = H_3 - \frac{1}{2}a(I_z^{(1)} - j_z^{(1)})^2$ rather than H_3, as is seen from (2.36).] In any case, one arrives at the result

$$\begin{aligned} Z &= -(\tfrac{1}{2}I)^{1/2}(E^2 - \omega^2)(DM_3)^{-1}\,, \\ Z_{12} &= k\omega^2(E+\omega)(E+2\omega)(DM_3)^{-1}\,, \\ Z_{34} &= -k\omega^2(E-\omega)(E-2\omega)(DM_3)^{-1}\,, \end{aligned} \tag{A4}$$

where k is defined by (2.38), and the abbreviation

$$E = E_+ + E_- \tag{A5}$$

is used. The parameter M_3 is given by

$$M_3^{-1} = a\left[1 - \frac{\omega(E^2 - \omega^2)}{D + \omega(E^2 - \omega^2)}\right], \tag{A6}$$

where

$$D = I(E^2 - \omega^2) - 2k^2\omega^3[(E+\omega)(E+2\omega)^2 + (E-\omega)(E-2\omega)^2]\,. \tag{A7}$$

The vibrational frequencies $\omega_{3\sigma}$ and the phonon operators (2.47) may be obtained with the usual RPA techniques. With the notation $b_1^\dagger = b^\dagger$, $b_2^\dagger = B^\dagger_{12}$, $b_3^\dagger = B^\dagger_{34}$, H_3 may be written in the form

$$H_3 = \text{constant} + \sum_{ij} \mathcal{A}_{ij} b_i^\dagger b_j + \frac{1}{2}\sum_{ij}(\mathcal{B}_{ij} b_i^\dagger b_j^\dagger + \text{H.c.})\,,$$

where $\underline{\mathcal{A}}$ and $\underline{\mathcal{B}}$ are real symmetric matrices. The equation $[H_3, \mathcal{O}^\dagger_{3\sigma}] = \omega_{3\sigma}\mathcal{O}^\dagger_{3\sigma}$ is equivalent to the usual RPA equations

$$\begin{aligned} \underline{\mathcal{A}}X(3\sigma) - \underline{\mathcal{B}}Y(3\sigma) &= \omega_{3\sigma}X(3\sigma)\,, \\ \underline{\mathcal{B}}X(3\sigma) - \underline{\mathcal{A}}Y(3\sigma) &= \omega_{3\sigma}Y(3\sigma)\,. \end{aligned}$$

The dimension of the eigenvalue problem can be halved by the well-known device of adding and subtracting the pair of equations leading to

$$\begin{aligned}(\underline{\mathcal{A}}-\underline{\mathcal{B}})[X(3\sigma)+Y(3\sigma)]&=\omega_{3\sigma}[X(3\sigma)-Y(3\sigma)],\\(\underline{\mathcal{A}}+\underline{\mathcal{B}})[X(3\sigma)-Y(3\sigma)]&=\omega_{3\sigma}[X(3\sigma)+Y(3\sigma)],\end{aligned}\tag{A8}$$

and finally

$$\begin{aligned}(\underline{\mathcal{A}}+\underline{\mathcal{B}})(\underline{\mathcal{A}}-\underline{\mathcal{B}})[X(3\sigma)+Y(3\sigma)]&=\omega_{3\sigma}{}^2[X(3\sigma)+Y(3\sigma)],\\(\underline{\mathcal{A}}-\underline{\mathcal{B}})(\underline{\mathcal{A}}+\underline{\mathcal{B}})[X(3\sigma)-Y(3\sigma)]&=\omega_{3\sigma}{}^2[X(3\sigma)+Y(3\sigma)].\end{aligned}\tag{A9}$$

Either one of the two eigenvalue equations (A9), which only involve a 3×3 matrix, may be solved for the $\omega_{3\sigma}$ and $X\pm Y$, while (A8) can be used to provide the complementary combination $X\mp Y$ for $\omega_{3\sigma}\neq0$.

In addition to the zero-frequency solution, one obtains the roots

$$\omega_{3\sigma}{}^2=\tfrac{1}{2}[b\pm(b^2-4c)^{1/2}],\tag{A10}$$

with

$$\begin{aligned}b&=2(E^2+\omega^2)+4ak^2E(E^2-2\omega^2)(E^2-4\omega^2),\\c&=(E^2-\omega^2)^2+4ak^2E(E^2-\omega^2)(E^2+2\omega^2)(E^2-4\omega^2).\end{aligned}\tag{A11}$$

The corresponding eigenvectors are given by

$$\begin{aligned}-X(3\sigma)(\omega+\omega_{3\sigma})&=Y(3\sigma)(\omega-\omega_{3\sigma})=(\tfrac{1}{2}I)^{1/2}\mathfrak{N}_\sigma,\\-X_{12}(3\sigma)(E-\omega-\omega_{3\sigma})&=Y_{12}(3\sigma)(E-\omega+\omega_{3\sigma})\\&=k(E-\omega)(E+2\omega)\mathfrak{N}_\sigma,\\X_{34}(3\sigma)(E+\omega-\omega_{3\sigma})&=-Y_{34}(3\sigma)(E+\omega+\omega_{3\sigma})\\&=k(E+\omega)(E-2\omega)\mathfrak{N}_\sigma,\end{aligned}\tag{A12}$$

where $\mathfrak{N}_\sigma$ is a normalization factor obtained from the condition

$$\begin{aligned}X^2(3\sigma)+X_{12}{}^2(3\sigma)+X_{34}{}^2(3\sigma)\\-Y^2(3\sigma)-Y_{12}{}^2(3\sigma)-Y_{34}{}^2(3\sigma)=1.\end{aligned}\tag{A13}$$

The zero-point energy $\mathcal{E}_3(\mathrm{zp})$ is obtained by expressing H_3 in the normal-ordered diagonal form (2.46). The result is

$$\begin{aligned}\mathcal{E}_3(\mathrm{zp})&=\tfrac{1}{2}a\{I+k^2(E+2\omega)^2[(E-\omega)^2+\omega^2]+k^2(E-2\omega)^2[(E+\omega)^2+\omega^2]\}\\&\quad-\sum_{\sigma=1}^{2}\omega_{3\sigma}\sum_i|Y_i(3\sigma)|^2-\tfrac{1}{4}[I+4k^2\omega^2(E^2+4\omega^2)]M_3{}^{-1}.\end{aligned}\tag{A14}$$

The last term in (A14) is just $-\frac{1}{2}\langle(I_z^{(1)}-j_z^{(1)})^2/M_3\rangle_\omega$, $\langle\ \rangle_\omega$ denoting the expectation value with respect to the Hartree-Bogoliubov vacuum. It is a correction arising from the presence of the zero-frequency mode.

Next, we take up the diagonalization of H_4. The two cases, $\Delta\neq0$ and $\Delta=0$ must be considered separately. If $\Delta\neq0$, the identity (2.42) holds and there is a zero-frequency mode, the pairing rotation, corresponding to Eq. (2.49). The number operator in the RPA is given by

$$\hat{N}\approx2\Omega+\hat{N}^{(1)}=2\Omega-\left[\frac{2\Delta^2}{GE}\right]^{1/2}(B_{14}^\dagger+B_{14}+B_{23}^\dagger+B_{23}).\tag{A15}$$

The gauge angle ϕ canonically conjugate to $\hat{N}^{(1)}$ is found by solving the equation

$$[H_4,\phi]=-iM_4{}^{-1}\hat{N}^{(1)}\tag{A16}$$

and has the simple form

$$\phi=\frac{i}{4}\left[\frac{GE}{2\Delta^2}\right]^{1/2}(B_{14}^\dagger-B_{14}+B_{23}^\dagger-B_{23}).\tag{A17}$$

The inertial parameter for pairing rotation M_4 then turns out to be

$$M_4=\frac{8\Delta^2}{GE^2}.\tag{A18}$$

The genuine vibrational modes can be obtained by the same technique applied to H_3. However, it turns out to be more convenient to proceed in a different manner. First, one observes that in the space of the B_{14}, B_{23} bosons there exists an obvious canonical pair of variables commuting with $\hat{N}^{(1)}$ and ϕ, given by

$$\begin{aligned}Q_3&=\tfrac{1}{2}E^{-1/2}(B_{14}^\dagger+B_{14}-B_{23}^\dagger-B_{23}),\\P_3&=\tfrac{1}{2}iE^{1/2}(B_{14}^\dagger-B_{14}-B_{23}^\dagger+B_{23}).\end{aligned}\tag{A19}$$

It is also convenient to introduce the following canonical variables:

$$\begin{aligned}Q_1&=\tfrac{1}{2}E_+{}^{-1/2}(B_{24}^\dagger+B_{24}),\quad P_1=iE_+{}^{1/2}(B_{24}^\dagger-B_{24}),\\Q_2&=\tfrac{1}{2}E_-{}^{-1/2}(B_{13}^\dagger+B_{13}),\quad P_2=iE_-{}^{1/2}(B_{13}^\dagger-B_{13}).\end{aligned}\tag{A20}$$

This provides a complete set of commuting pairs,

in terms of which H_4 takes the form

$$H_4 = -2E + \tfrac{1}{2}\hat{N}^{(1)2}/M_4 + \frac{1}{2}\sum_{i=1}^{3} P_i^2 + \frac{1}{2}\sum_{i,j=1}^{3} K_{ij}Q_iQ_j\,, \tag{A21}$$

where K is a real symmetric matrix defined as follows:

$$\begin{aligned}
K_{11} &= 4E_+^2 + 3\epsilon^2\Omega E_+^{-1}(a - 2G\Delta^2\gamma^{-2})\,,\\
K_{12} &= -3\epsilon^2\Omega(E_+E_-)^{-1/2}(a + 2G\Delta^2\gamma^{-2})\,,\\
K_{13} &= -\Delta(6G\Omega)^{1/2}\epsilon^2\gamma^{-2}E_+^{-1/2}E\,,\\
K_{22} &= 4E_-^2 + 3\epsilon^2\Omega E_-^{-1}(a - 2G\Delta^2\gamma^{-2})\,,\\
K_{23} &= -\Delta(6G\Omega)^{1/2}\epsilon^2\gamma^{-2}E_-^{-1/2}E\,,\\
K_{33} &= 4\Delta^2E^2\gamma^{-2}\,.
\end{aligned} \tag{A22}$$

The diagonalization of H_4 reduces to the simple task of diagonalizing the potential-energy quadratic form. This is accomplished by introducing a new set of coordinates $\mathcal{Q}_\sigma$ and canonically conjugate momenta $\mathcal{P}_\sigma$, where

$$\begin{aligned}
\mathcal{Q}_\sigma &= \sum_{i=1}^{3} C_{i\sigma}Q_i\,,\\
\mathcal{P}_\sigma &= \sum_{i=1}^{3} C_{i\sigma}P_i\,,
\end{aligned} \tag{A23}$$

in terms of which H_4 takes the diagonal form

$$H_4 = -2E + \tfrac{1}{2}\hat{N}^{(1)2}/M_4 + \frac{1}{2}\sum_{i=1}^{3}(\mathcal{P}_\sigma^2 + \omega_{4\sigma}^2\mathcal{Q}_\sigma^2)\,. \tag{A24}$$

The diagonalization of the potential energy leads to the eigenvalue problem

$$\sum_{j=1}^{3} K_{ij}C_{j\sigma} = \omega_{4\sigma}^2 C_{i\sigma}\,; \quad i = 1,2,3 \tag{A25}$$

and the kinetic energy is automatically diagonal if the eigenvectors are normalized. Since the $\omega_{4\sigma}^2$ are roots of a cubic equation, we shall not bother to write them out explicitly.

The normal-mode bosons $\mathcal{O}_{4\sigma}$, $\mathcal{O}_{4\sigma}^\dagger$ may then be defined in the usual way:

$$\begin{aligned}
\mathcal{Q}_\sigma &= (2\omega_{4\sigma})^{-1/2}(\mathcal{O}_{4\sigma}^\dagger + \mathcal{O}_{4\sigma})\,,\\
\mathcal{P}_\sigma &= i(\omega_{4\sigma}/2)^{1/2}(\mathcal{O}_{4\sigma}^\dagger - \mathcal{O}_{4\sigma})\,.
\end{aligned} \tag{A26}$$

In terms of these, H_4 takes the form

$$H_4 = -2E + \frac{1}{2}\sum_{\sigma=1}^{3}\omega_{4\sigma} + \sum_{\sigma=1}^{3}\omega_{4\sigma}\mathcal{O}_{4\sigma}^\dagger\mathcal{O}_{4\sigma}\,. \tag{A27}$$

The zero-point energy is then explicitly given by

$$\mathcal{E}_4(\mathrm{zp}) = -2E + \frac{1}{2}\sum_{\sigma=1}^{3}\omega_{4\sigma}\,. \tag{A28}$$

The contribution of the pairing rotation is

$$-\tfrac{1}{2}\langle\hat{N}^{(1)2}/M_4\rangle_\omega = -\tfrac{1}{4}E\,.$$

The X's and Y's in (2.51) may be obtained in terms of the $C_{i\sigma}$ by combining the transformations (A26), (A23), (A20), and (A19). The result is:

$$\begin{aligned}
X_{24}(4\sigma) &= \tfrac{1}{2}(2E_+\omega_{4\sigma})^{-1/2}(2E_+ + \omega_{4\sigma})C_{1\sigma}\,,\\
Y_{24}(4\sigma) &= -\tfrac{1}{2}(2E_+\omega_{4\sigma})^{-1/2}(2E_+ - \omega_{4\sigma})C_{1\sigma}\,,\\
X_{13}(4\sigma) &= \tfrac{1}{2}(2E_-\omega_{4\sigma})^{-1/2}(2E_- + \omega_{4\sigma})C_{2\sigma}\,,\\
Y_{13}(4\sigma) &= -\tfrac{1}{2}(2E_-\omega_{4\sigma})^{-1/2}(2E_- - \omega_{4\sigma})C_{2\sigma}\,,
\end{aligned} \tag{A29a}$$

$$\begin{aligned}
X_{14}(4\sigma) &= -X_{23}(4\sigma) = \tfrac{1}{2}(2E\omega_{4\sigma})^{-1/2}(E + \omega_{4\sigma})C_{3\sigma}\,,\\
Y_{14}(4\sigma) &= -Y_{23}(4\sigma) = -\tfrac{1}{2}(2E\omega_{4\sigma})^{-1/2}(E - \omega_{4\sigma})C_{3\sigma}\,.
\end{aligned} \tag{A29b}$$

Finally, take the case $\Delta = 0$. Then, H_4 breaks up into two disjoint quadratic forms:

$$H_4 = H_4(\mathrm{pp}) + H_4(\mathrm{ph})\,, \tag{A30}$$

where $H_4(\mathrm{pp})$ is the pair-vibrational Hamiltonian describing the transfer or removal of a pair of particles, and $H_4(\mathrm{ph})$ describes particle-hole excitations. Explicitly, these are given by

$$H_4(\mathrm{pp}) = E(B_{14}^\dagger B_{14} + B_{23}^\dagger B_{23}) - GP^{(1)\dagger}P^{(1)} \tag{A31}$$

and

$$H_4(\mathrm{ph}) = 2E_+B_{24}^\dagger B_{24} + 2E_-B_{13}^\dagger B_{13} + \tfrac{1}{2}aj_x^{(1)2}\,, \tag{A32}$$

in which $P^{(1)}$ is the $\Delta = 0$ limit of (2.41), and

$$E_\pm = (\epsilon^2 + \omega^2 \pm \omega\epsilon)^{1/2}\,. \tag{A33}$$

First consider the pair-vibrational branch. Since $\hat{N}^{(1)} = 0$ when $\Delta = 0$, there is no zero-frequency mode. Nevertheless, it is useful to introduce the following canonical variables analogous to (A15), (A17), and (A19):

$$\begin{aligned}
Q_3 &= \tfrac{1}{2}E^{-1/2}(B_{14}^\dagger + B_{14} - B_{23}^\dagger - B_{23})\,,\\
P_3 &= \tfrac{1}{2}iE^{1/2}(B_{14}^\dagger - B_{14} - B_{23}^\dagger + B_{23})\,,\\
Q_4 &= -\tfrac{1}{2}iE^{-1/2}(B_{14}^\dagger - B_{14} + B_{23}^\dagger - B_{23})\,,\\
P_4 &= \tfrac{1}{2}E^{1/2}(B_{14}^\dagger + B_{14} + B_{23}^\dagger + B_{23})\,.
\end{aligned} \tag{A34}$$

When expressed in terms of these variables, $H_4(\mathrm{pp})$ is immediately in diagonal form:

$$\begin{aligned}
H_4(\mathrm{pp}) &= -E + \tfrac{1}{2}[P_3^2 + P_4^2 + \omega_p^2(Q_3^2 + Q_4^2)]\\
&= -E + \omega_p + \omega_p(\mathcal{O}_{43}^\dagger\mathcal{O}_{43} + \mathcal{O}_{44}^\dagger\mathcal{O}_{44})\,,
\end{aligned} \tag{A35}$$

where the pair-vibration excitation energy is given by

$$\omega_p = \omega_{43} = \omega_{44} = E\left[1 - \frac{G\Omega}{2\epsilon}\left(\frac{\epsilon+2\omega}{E_+} + \frac{\epsilon-2\omega}{E_-}\right)\right]^{1/2}. \tag{A36}$$

It is clear from the gap equation (2.24) that $\omega_p \to 0$ at the transition point from the normal to the superconducting solution, signaling a switch from the pair-vibrational to the pair-rotational scheme. The degeneracy in (A36) means that the excitation energy is equal for the two-particle and the two-hole transfer processes. Because of the degeneracy, the operators $\mathcal{O}_{4\sigma}$, $\mathcal{O}^\dagger_{4\sigma}$ are not uniquely defined, but we shall not need these in the present work.

To diagonalize $H_4(\mathrm{ph})$, it is convenient to again perform the canonical transformation (A20). The result is

$$H_4(\mathrm{ph}) = -E + \tfrac{1}{2}(P_1^2 + P_2^2) + \tfrac{1}{2}(u_+ Q_1^2 + u_- Q_2^2 + 2vQ_1Q_2), \tag{A37}$$

where

$$u_\pm = 4E_\pm^2 + 3a\epsilon^2\Omega E_\pm^{-1}, \qquad v = -3a\epsilon^2\Omega(E_+E_-)^{-1/2}. \tag{A38}$$

The quadratic form is easily diagonalized by the canonical transformation

$$\mathcal{Q}_1 = \cos\theta Q_1 + \sin\theta Q_2, \quad \mathcal{P}_1 = \cos\theta P_1 + \sin\theta P_2,$$
$$\mathcal{Q}_2 = -\sin\theta Q_1 + \cos\theta Q_2, \quad \mathcal{P}_2 = -\sin\theta P_1 + \cos\theta P_2. \tag{A39}$$

In terms of these variables,

$$H_4(\mathrm{ph}) = -E + \frac{1}{2}\sum_{\sigma=1}^{2}(\mathcal{P}_\sigma^2 + \omega_{4\sigma}^2\mathcal{Q}_\sigma^2), \tag{A40}$$

where the frequencies are given by

$$\omega_{4\sigma}^2 = \tfrac{1}{2}\{u_+ + u_- \pm [(u_+ - u_-)^2 + 4v^2]^{1/2}\} \tag{A41}$$

and

$$\cos^2\theta = \tfrac{1}{2}\{1 + (u_+ - u_-)[(u_+ - u_-)^2 + 4v^2]^{-1/2}\}. \tag{A42}$$

The phonon operators may be defined by (A26). Then (A40) takes the form

$$H_4(\mathrm{ph}) = -E + \frac{1}{2}\sum_{\sigma=1}^{2}\omega_{4\sigma} + \sum_{\sigma=1}^{2}\omega_{4\sigma}\mathcal{O}^\dagger_{4\sigma}\mathcal{O}_{4\sigma}. \tag{A43}$$

The X and Y amplitudes have the form of (A29a) with $c_{11} = c_{22} = \cos\theta$, $c_{12} = -c_{21} = \sin\theta$.

From (A35) and (A43), we see that the total zero-point energy for the $\Delta = 0$ case is given by

$$\mathcal{E}_4(\mathrm{zp}) = -2E + \frac{1}{2}\sum_{\sigma=1}^{4}\omega_{4\sigma}. \tag{A44}$$

---

*Work supported by the National Science Foundation, the U. S. Atomic Energy Commission, and the Deutsche Forschungsgemeinschaft.

†Permanent address: Department of Physics, University of Notre Dame, Notre Dame, Indiana 46556.

‡Permanent address: Technische Universität München, 8046 Garching, West Germany.

§Permanent address: Department of Mathematical Physics, Lund Institute of Technology, Lund, Sweden.

[1]See the review articles: R. A. Sorensen, Rev. Mod. Phys. 45, 353 (1973); A. Johnson and Z. Szymański, Phys. Rep. 7, 181 (1973), and references therein.

[2]B. Banerjee, H. J. Mang, and P. Ring, Nucl. Phys. A215, 366 (1973); P. Ring, H. J. Mang, and B. Banerjee, *ibid.* A225, 141 (1974).

[3]K. Kumar, Phys. Scr. 6, 270 (1972).

[4]A. Goswami, L. Lin, and G. Struble, Phys. Lett. 25B, 53 (1967); L. Lin, Nuovo Cimento Lett. 11, 51 (1974); Yu. T. Grin, Phys. Lett. 52B, 135 (1974).

[5]E. R. Marshalek and J. Weneser, Phys. Rev. C 2, 1682 (1970); E. R. Marshalek, *ibid.* 1710 (1971); in Proceedings of the Conference on Vibrational Nuclei, Zagreb, Yugoslavia, September 24–27, 1974, invited paper.

[6]S. Bose, J. Krumlinde, and E. R. Marshalek, Phys. Lett. 53B, 136 (1974).

[7]It will be seen that the R(8) model is unsuited for testing projection of angular momentum.

[8]J. Krumlinde and Z. Szymański, Ann. Phys. (N.Y.) 79, 201 (1973).

[9]A. L. Goodman, Nucl. Phys. A230, 466 (1974).

[10]SCC1 is identical for the two-dimensional R(6) and the three-dimensional R(8) models.

[10(a)]This implies the existence of isomer traps below the yrast line in this model.

[11]E. R. Marshalek, Nucl. Phys. A224, 221 (1974).

[12]E. R. Marshalek, Phys. Rev. C 11, 1426 (1975).

[13]B. Mottelson, in proceedings of the Nuclear Structure Symposium of the Thousand Lakes, Joutsa, 1970 [Nordita publication, No. 417 (unpublished)].

[14]E. R. Marshalek and J. Weneser, Ann. Phys. (N.Y.) 53, 569 (1969).

[15]A. Faessler, F. Grümmer, L. Lin, and J. Urbano, Phys. Lett. 48B, 87 (1974).

[16]K. Dietrich, H. Mang, and J. Pradal, Phys. Rev. 135, B22 (1964).

[17]In Ref. 8, the notation $T^{12}_{0\mu} = Q_{2\mu}$ is used.

[18]The matrix dimension $= (\Omega+5)!/(120\times\Omega!)$.

[19]M. Sano, T. Takemasa, and M. Wakai, Nucl. Phys. A190, 471 (1972).

[20]R. A. Lyttleton, *The Stability of Rotating Liquid Masses* (Cambridge U.P., Cambridge, 1953).